Aerospace Science and Technology 142 (2023) 108597

Contents lists available at ScienceDirect

Aerospace Science and Technology

journal homepage: www.elsevier.com/locate/aescte

On quantifying uncertainty in lightning strike damage of composite laminates: A hybrid stochastic framework of coupled transient thermal-electrical simulations

R.S. Chahar [a], J. Lee [b], T. Mukhopadhyay [c,*]

[a] Department of Aerospace Engineering, Indian Institute of Technology Kanpur, Kanpur, India
[b] Department of Mechanical and Aerospace Engineering, Utah State University, Logan, USA
[c] School of Engineering, University of Southampton, Southampton, UK

ARTICLE INFO

Article history:
Received 13 April 2023
Received in revised form 25 August 2023
Accepted 25 August 2023
Available online 31 August 2023
Communicated by Sirish Namilae

Keywords:
Uncertainty quantification
Lightning strike damage
Composite laminates
Support vector machine regression
Global sensitivity analysis
Coupled transient thermal-electrical simulations

ABSTRACT

Lightning strike damage can severely affect the thermo-mechanical performance of composite laminates. It is essential to quantify the effect of lightning strikes considering the inevitable influence of material and geometric uncertainties for ensuring the operational safety of aircraft. This paper presents an efficient support vector machine (SVM)-based surrogate approach coupled with computationally intensive transient thermal-electrical finite element simulations to quantify the uncertainty in lightning strike damage. The uncertainty in epoxy matrix thermal damage and electrical responses of unprotected carbon/epoxy composite laminates is probabilistically quantified considering the stochasticity in temperature-dependent multi-physical material properties and ply orientations. Further, the SVM models are exploited for variance-based global sensitivity analysis to investigate the input parameters' relative influence on the lightning strike-induced damage behavior. Due to the adoption of a coupled SVM-based simulation approach here, it has become possible to carry out a comprehensive uncertainty quantification leading to complete probabilistic descriptions of the electrical and lightning damage parameters despite the requirement of performing a large number of computationally intensive function evaluations. The results reveal that source-uncertainty of the unprotected laminates significantly influences the epoxy matrix decomposition, electrical current density and electric potential, wherein longitudinal electrical conductivity is most sensitive to stochastic variations followed by other electrical, thermal and geometric parameters.

1. Introduction

Lightning strike-induced damage poses a serious natural threat to aircraft flight safety [1,2]. Such damage in aircraft can differ depending on its damage sources and mechanisms: *i*) thermal damage involving intense and highly localized heat sources (i.e., Joule heat and convective/radiative flux) and *ii*) dynamic mechanical damage resulting from associated plasma-charged particles interacting with incident/external electromagnetic fields (i.e., shock-wave overpressure, Lorentz force). Thermal damage from lightning strikes on composite components of aircraft is mainly due to the high orthotropic electric resistive heating [3–8]. Although involved with complex plasma physics and electromagnetic interactions, lightning mechanical damage is often minimal and less significant than lightning thermal damage, thus it is often ignored.

Physical damage to the fiber-reinforced polymeric (FRP) composites at the lightning strike area involves intense fiber failure/splitting, widespread matrix cracking/decomposition/ablation, and inter- and intra-ply delamination. Protection of aircraft composite structures and flight safety remains a challenge from lightning strike damage even after employing anti-lightning strike devices. In this article, for ensuring adequate operational flight safety, we would quantify lightning strike damage probabilistically accounting for the effect of inevitable source-uncertainties. This will allow us to develop an improved design paradigm through inclusive analysis and design of aircraft structures considering probabilistic information to avert catastrophic structural failure and further assessment of residual structural performance.

Fig. 1(A) provides three lightning strike zones of a typical aircraft, depending on their probability of occurrence and severity: *Zone 1* - High possibility of initial lightning attachment, *Zone 2* - High possibility of lightning being moved away from the initial attachment point (swept stroke), and *Zone 3* – Parts of the aircraft

* Corresponding author.
E-mail address: T.Mukhopadhyay@soton.ac.uk (T. Mukhopadhyay).

https://doi.org/10.1016/j.ast.2023.108597

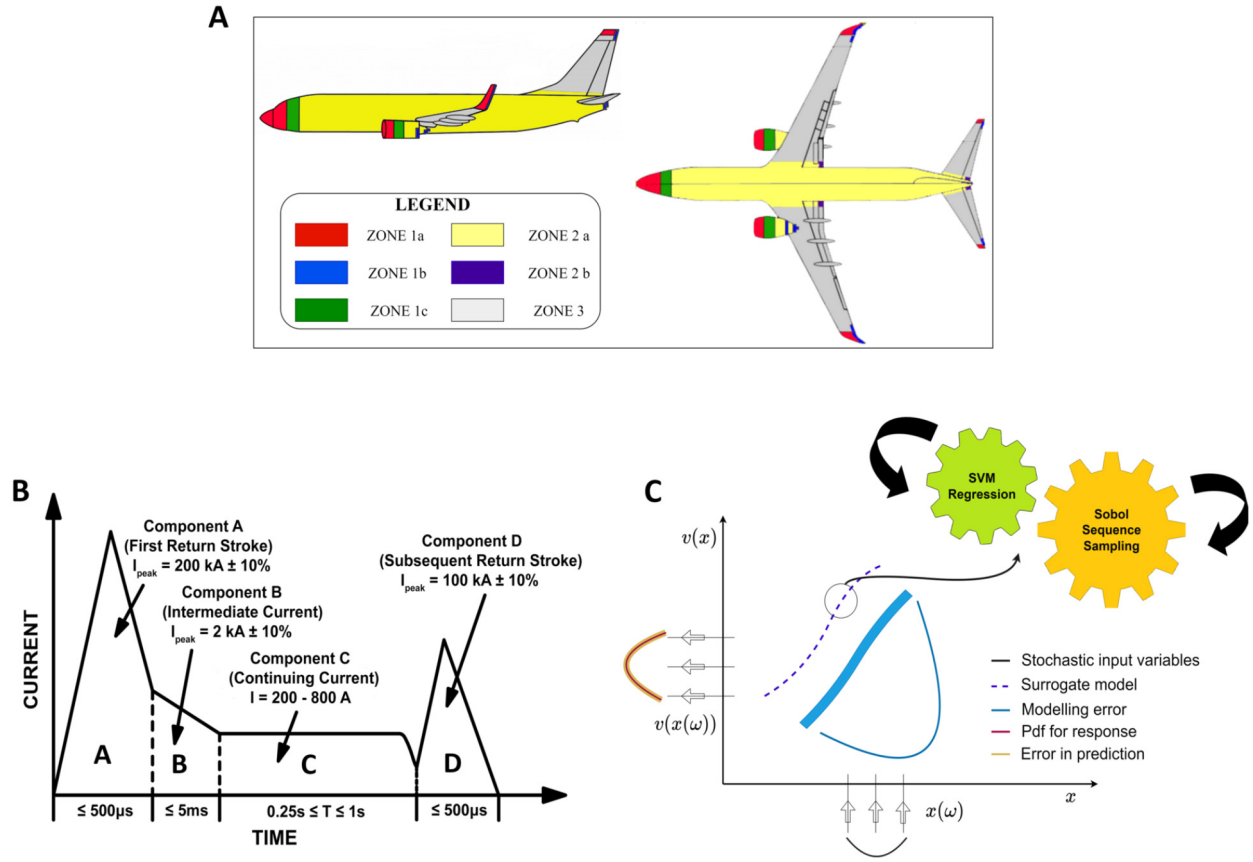

Fig. 1. Introductory overview of probabilistic characterization concerning lightening strike damage. (A) Standard lightning strike zones of an aircraft [11]. **(B)** Lightning current waveform components A, B, C and D showing peak amplitudes and time durations [12]. **(C)** A typical representation of surrogate-based stochastic analysis. Here $x(\omega))$ and $v(x(\omega))$ are the vectors of stochastic input parameters and stochastic responses respectively, wherein ω denotes the stochastic character.

which experience currents without a lightning strike. As evident from the figure, *Zone 2* covers most external aircraft surfaces. Four current components of the standard lightning current waveform are shown in Fig. 1(B). Component A is the first return stroke. This component is followed by an intermediate current component B of longer duration and lower magnitude. Continuing current Component C follows component B and it has an even lower amplitude and longer duration. Component D is a re-strike. Due to relatively high peak current amplitudes, Components A and B are typically used in physical lightning damage assessment. Many experimental studies are reported on the characterization of the damages that occur due to lightning strikes on carbon fiber-reinforced composite laminates by tailoring the impulse current waveform parameters [3,4,9,10]. We provide a brief review of the lightning strike effect on composite laminates following primarily a deterministic framework in the following paragraph.

Feraboli et al. [3] performed a series of artificial lightning strike tests at different current amplitudes to understand the lightning damage resistance of composite laminates. The presence of metallic fasteners in the skin significantly affected the lightning damage in the laminate and its residual strength. Hirano et al. [4] performed experiments concerning lightning strikes on graphite/epoxy composite laminates for different current waveforms parameters. The effects of electrical charges, action integrals and peak current amplitudes were investigated on the lightning damage that occurred in carbon/epoxy laminates and different damage modes such as fiber damage, epoxy matrix thermal decomposition, and delamination were noticed. They found that the electrical conductivities have a strong effect on the thermal damage of carbon/epoxy composite laminates and lightning damage can be reduced by improving laminate electrical conductivity. Ogasawara et al. [6] developed a coupled thermal-electrical ABAQUS model to predict damage from a lightning strike and validated with the experimental work done by Hirano et al. [4]. The proposed model was developed using room-temperature material properties for carbon/epoxy laminate, capable of estimating the extent and shape of in-plane lightning thermal damage areas and through-the-thickness damage development. This work assumed the linear variation of through-thickness electrical conductivity as a function of temperature in the range from epoxy decomposition temperature to carbon sublimation temperature. Abdelal and Murphy [13] predicted the lightning thermal damage in baseline (unprotected) and copper mesh protected carbon/epoxy laminates using temperature-dependent material properties. Several subroutines were used to calculate the degree of epoxy matrix thermal decomposition and internal heat generation resulting from a lightning strike. The model proposed in this work clearly showed that the presence of conductive metallic mesh mitigates lightning damage to the underlying carbon/epoxy laminate. Dong et al. [14] numerically analyzed the effects of the lightning current waveform parameters on the lightning damage area, lightning damage volume and lightning damage depth. Wang et al. [15] used different aluminum coatings on the composite laminates to design a protection system for the lightning strike and compared the results with the unprotected laminates. The aluminum coating was found to be an effective protective layer to be used as an anti-lightning strike arrangement. Lee et al. [16] evaluated the lightning protection performance of pitch-based carbon fiber paper (PCFP) and copper mesh (CM) outer layer. Epoxy matrix thermal decomposition, indicative of lightning thermal damage, was characterized using temperature-dependent properties. The copper mesh was found to be an excellent protection system for composite laminates

allowing only the top carbon/epoxy layer to be damaged while with a PCFP outer layer, the thermal damage was up to the 3rd carbon/epoxy ply. This work noted that the lightning strike performance of a PCFP layer can be improved by tailoring carbon fiber volume fraction/orientation (leading to a huge increase in electrical conductivity), thus it can be used for a potential non-metallic lightning strike protection material. In the work of Lee et al. [17], lightning thermal damage in carbon/epoxy laminates was predicted with various matrix decomposition profiles (i.e., damage variation within decomposition temperatures). For instance, the extent of epoxy matrix decomposition was assumed to vary either linearly or quadratically throughout 300-500 °C and 300-600 °C. A linear damage approximation in the temperature ranges between 300 °C and 500 °C showed the best agreement with experimental observation. Shah and Lee [18] investigated the influence of randomly distributed voids and random electrical conductivity on the damage behavior of carbon/epoxy composites under lightning strike based on a limited number of realizations. They conducted two case studies for two different 40 kA current waveforms. In each case study, only nine simulations were performed with randomly generated and distributed electrical conductivities and voids (i.e., zero material properties). It was reported that electrical conductivity affects lightning thermal damage somewhat, whereas voids do not affect it much. However, there is a strong rationale to carry out further studies on uncertainty quantification and sensitivity analysis comprehensively in a probabilistic framework where thousands of simulations are required to be carried out corresponding to different random combinations of the stochastic lightning strike and composite material parameters. It has not been possible so far since each of the lightning strike simulations are computationally very expensive and it is practically impossible to perform Monte Carlo simulations based on thousands of finite element simulations concerning lightning strike damage prediction. In this work, we would overcome this by introducing support vector machine-based surrogate models in conjunction with the actual finite element simulations.

In general, since laminated composite structures are complex to manufacture according to exact material and geometric specifications [19,20] and the parameters involving the operational conditions during the service life of composites can vary widely, it is imperative to adopt a stochastic analysis approach for quantifying the associated uncertainties. Researchers have performed surrogate-based stochastic analyses to quantify the uncertain global responses in the fiber-reinforced composites (such as natural frequency, buckling, static deformation and progressive failure) considering the material and geometric properties uncertainty in the last decade [21–26]. However, uncertainty quantification of the lightning damage in composite laminates has not been thoroughly investigated yet. Earlier Shah and Lee [18] reported the results of nine random realizations only considering the variation of electrical conductivity without accounting for the interactions with other material and geometric properties. While the computationally intensive nature of each realization restricts a large number of direct finite element simulations, the variations reported in the paper create a strong case for performing a full-scale probabilistic analysis concerning lightning strike damage in composite laminates. Following a comprehensive probabilistic framework, this paper aims to present the uncertainty quantification of in-plane and out-of-plane lightning thermal damage in unprotected carbon/epoxy laminates based on stochastic temperature-dependent material properties and ply orientations. A finite element (FE) model of fully coupled transient thermal-electrical analysis would be developed to provide uncertainty estimates for the lightning thermal damage in the laminates. The deterministic model predictions would be compared with the experimental results of Hirano et al. [4], and FE model results of Ogasawara et al. [6] and Lee et al. [16] for establishing adequate confidence in the baseline FE model. To mitigate the computationally intensive nature of Monte Carlo simulation-assisted probabilistic analysis using exorbitantly expensive FE simulations of lightning strike, we would develop a hybrid stochastic framework by coupling support vector machine (SVM) based surrogates [27,28] therein. Quasi-random Sobol sequence algorithm [29,30] would be adopted to train the machine learning models (i.e. computationally efficient surrogates of the expensive finite element simulations) efficiently (refer to Fig. 1(C)). Subsequently, the probabilistic uncertainty quantification and global sensitivity analysis would be carried out based on the machine learning models considering stochasticity in multi-physical material properties and geometric parameters.

The remainder of this article is organized as follows: Section 2 describes the FE modeling for transient thermal-electrical analysis of lightning strike damage and its validation with deterministic models; Section 3 discusses preliminary screening of important parameters for stochastic analysis; Section 4 explains SVM based surrogate modeling approach that is coupled subsequently with the FE model for carrying out Monte Carlo simulations and variance-based global sensitivity analysis; Section 5 presents numerical results for uncertainty quantification and global sensitivity analysis of lightning damage; Section 6 presents concluding remarks.

2. Finite element modeling for lightning strike analysis

2.1. Description of the finite element model

In this study, a baseline FE model is developed consisting of a transient coupled thermal-electrical analysis (30 μs), followed by a transient heat transfer analysis (10s). The FE code ABAQUS is used to simulate the lighting thermal damage in a 32-ply carbon/epoxy laminate with quasi-isotropic lay-up of $([45/0/-45/90])_{4S}$. The ply thickness is 0.125 mm, leading to the total laminate thickness of 4 mm. The simulated laminate is 100 mm in width and 150 mm in length. Each carbon/epoxy laminae are meshed using three-dimensional 8-node linear coupled thermal-electric brick (DC3D8E) elements. As the effect of lightning damage is negligible after top 16 plies, top 16 plies are taken as orthotropic and remaining 16 plies are taken as quasi-isotropic (modeled using single DC3D8E element). Note that the temperature increase in the inner plies is minor compared to the outer plies. Thus, the implementation of a single quasi-isotropic layer, equivalent to 16 orthotropic layers for the bottom half, is computationally efficient while maintaining the same level of modeling accuracy [16]. The total number of finite elements used in the model is 43200, as finalized based on a mesh convergence study [16].

Electrical and thermal boundary conditions imposed on AS4/3506a laminate are shown in Fig. 2(A) and Fig. 2(B) for coupled thermal electric and subsequent heat transfer analysis respectively. The bottom surface of the laminate is electrically grounded by applying zero electrical potentials on the lateral and bottom surfaces. Thermal radiation, with a surface emissivity of 0.85 and the ambient temperature of 25 °C, is imposed on the top and lateral surfaces of the laminate whereas the bottom surface is adiabatic during all simulations. Thermal convection becomes more intense during thermal equilibrium. Thus, thermal convection with a coefficient 200 $W/m^2/K$ is imposed on the laminate's top and lateral surfaces only during subsequent heat transfer analysis.

In this study, a 10 mm diameter arc channel, typically corresponding to a 40kA peak current amplitude, is used in all lightning strike simulations. The red region in Fig. 2(A) and Fig. 2(B) indicates the initial lightning attachment region ($D = 10$ mm) used in the current FE model. In practice, the lightning arc channel expands and shrinks during its evolution stage. The rate of arc channel front evolution depends on the surface conductivity of a ma-

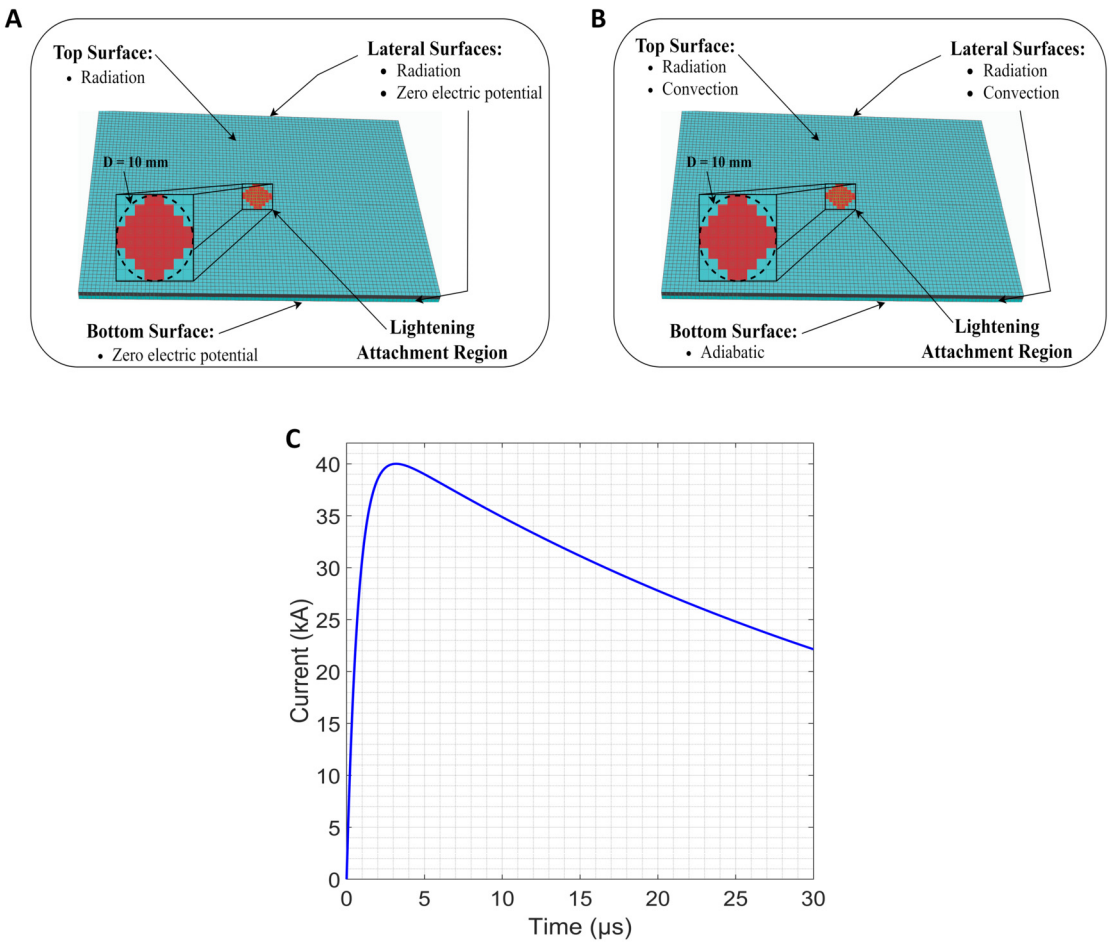

Fig. 2. Boundary conditions of the finite element model with component D current waveform. (A) Thermal and electrical boundary conditions imposed on unprotected 32-ply AS4/3506a laminate subjected to uniformly distributed surface current with 40 kA peak current amplitude of modified component D waveform in coupled thermal electric analysis. **(B)** Thermal and electrical boundary conditions imposed on the laminate in subsequent heat transfer analyses in lightning strike FE simulations. The red regions on the laminate top ply are lightning attachment regions and the black dotted circle is a lightning arc channel having a diameter of 10 mm. **(C)** Double exponential impulse current waveform. (For interpretation of the colors in the figure(s), the reader is referred to the web version of this article.)

Table 1
Material properties of AS4/3506a carbon/epoxy composite laminate [32–35].

Temp, T (°C)	Density, ρ^a (kg/mm^2)	Specific Heat, C_p^a (J/(kg.K))	Thermal Conductivity, k^a			Electrical Conductivity, σ^b		
			Long. (W/(mm.K))	Trans. (W/(mm.K))	Thick. (W/(mm.K))	Long. (S/mm)	Trans. (S/mm)	Thick. (S/mm)
25	1.52E-06	1065	466E-02	6.87E-04	6.87E-04	34.63	1.21E-03	3.23E-06
334	1.52E-06	2100	2.47E-02	3.728E-04	3.728E-04	34.63	1.21E-03	3.23E-06
500	1.1E-06	2100	1.463E-02	1.788E-04	1.788E-04	34.63	2	2
1000	1.1E-06	1900	1.172E-02	1.317E-04	1.317E-04	34.63	2	2
3316	1.1E-06	2509	1.00E-04	1.00E-04	1.00E-04	34.63	2	2
3367	1.1E-06[c]	5875[c]	1.00E-04[c]	1.00E-04[c]	1.00E-04[c]	1[c]	0.2[c]	1.0E+06[c]

[a] Refs. [32] and [33].
[b] Refs. [34] and [35].
[c] Extrapolated material properties over the temperature range (25 °C - 3316 °C).

terial, the magnitude of the peak current and temporal characteristics of an impulse waveform [31]. The incorporation of spatially- and temporally-varying arc channel can better characterize structural response and associated lightning damage, but drastically increases computational time. Therefore, the majority of lightning damage models available in the open literature assume that the arc channel planner area remains constant. There exists a trade-off between model accuracy and computational performance. As the primary focus of this paper is uncertainty analysis resulting from the inherent stochasticity, the effects of varying arc channel on lightning damage in composites are not considered in the current work. However, more accurate lightning strike modeling can be adopted in the future following a similar stochastic analysis framework as proposed here. A uniformly distributed surface current with 40 kA peak amplitude of modified component D waveform (as per SAE-ARP 5412 [11]) is applied over a 10 mm diameter arc channel. A double exponential impulse current waveform producing a 40 kA peak amplitude (refer to Fig. 2(C)) is implemented in a user-defined amplitude subroutine (UAMP) as follows:

$$I(t) = I_A(e^{-\hat{\alpha}t} - e^{-\hat{\beta}t}) \tag{1}$$

where $I_A = 43762$ A, $\hat{\alpha} = 22708$ 1/s, and $\hat{\beta} = 1294530$ 1/s.

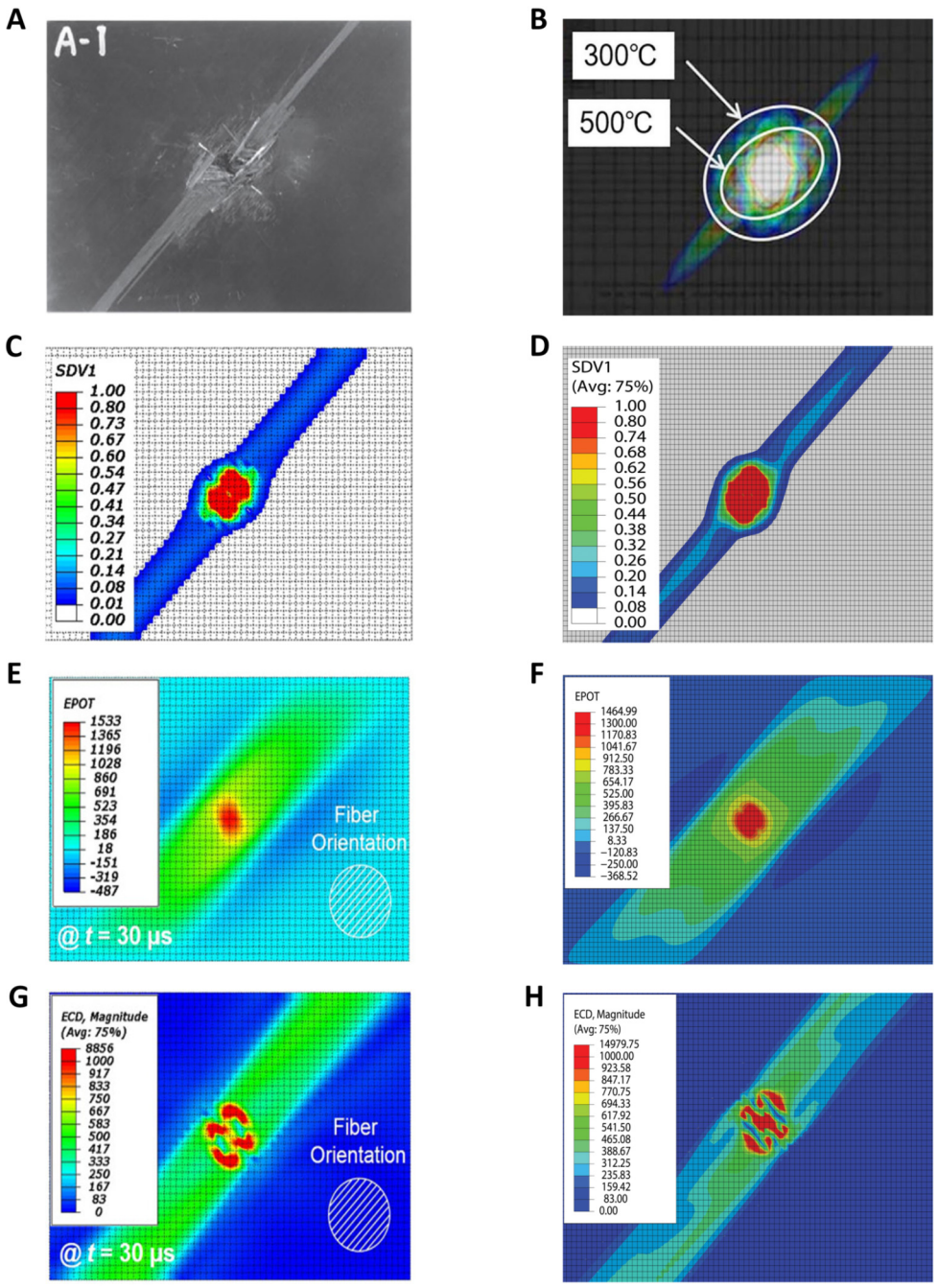

Fig. 3. Comparison between experimental and numerically predicted (literature and current FE model) lightning damage and electrical response in the outermost AS4/3506a layer. (A) Visual inspection from Hirano et al. [4] **(B, C, D)** Predicted matrix decomposition indicative of lightning thermal damage from Ogasawara et al. [6], Lee et al. [16], and the present FE model, respectively. In Fig. 3 (C) and 3 (D), SDV1 is the state variable used in the HETVAL user subroutine which represents the degree of thermal decomposition. **(E, F)** Electrical potential (EPOT) distributions from Lee et al. [16] and the current study, respectively. **(G, H)** Electrical current density (ECD) distributions from Lee et al. [16] and the present FE model, respectively. Note that the results from the current FE model are captured at the end of coupled thermal-electrical analysis (30 µs).

A user-defined heat generation subroutine (HETVAL) is developed to calculate the extent of epoxy matrix thermal decomposition at each time increment. The onset of matrix decomposition is assumed to start at 300 °C and vary linearly up to 500 °C. This indicates that the degree of matrix decomposition is 0 (undamaged at 300 °C) and 1 (fully damaged at 500 °C). The damaged material properties (due to irreversible permanent epoxy matrix damage) are updated using a user-defined field subroutine (USDFLD). Temperature-dependent orthotropic material properties for AS4/3506a laminate used in the present work are presented in Table 1.

2.2. Validation of deterministic lightning strike damage model

The experimental test results of Hirano et al. [4] and FE model results of Ogasawara et al. [6] and Lee et al. [16] are used to validate the current FE model. Fig. 3(A) shows the lightning damage in a composite laminate experimentally tested by Hirano et al. [4]. Fig. 3(B) and Fig. 3(C) show the matrix decomposition predicted by Ogasawara et al. [6] and Lee et al. [16] respectively. Fig. 3(D) shows the epoxy matrix decomposition predicted by the present FE model in the top ply of AS4/3506a carbon/epoxy laminate. In Fig. 3(B), thermal damage is defined in terms of temperature which

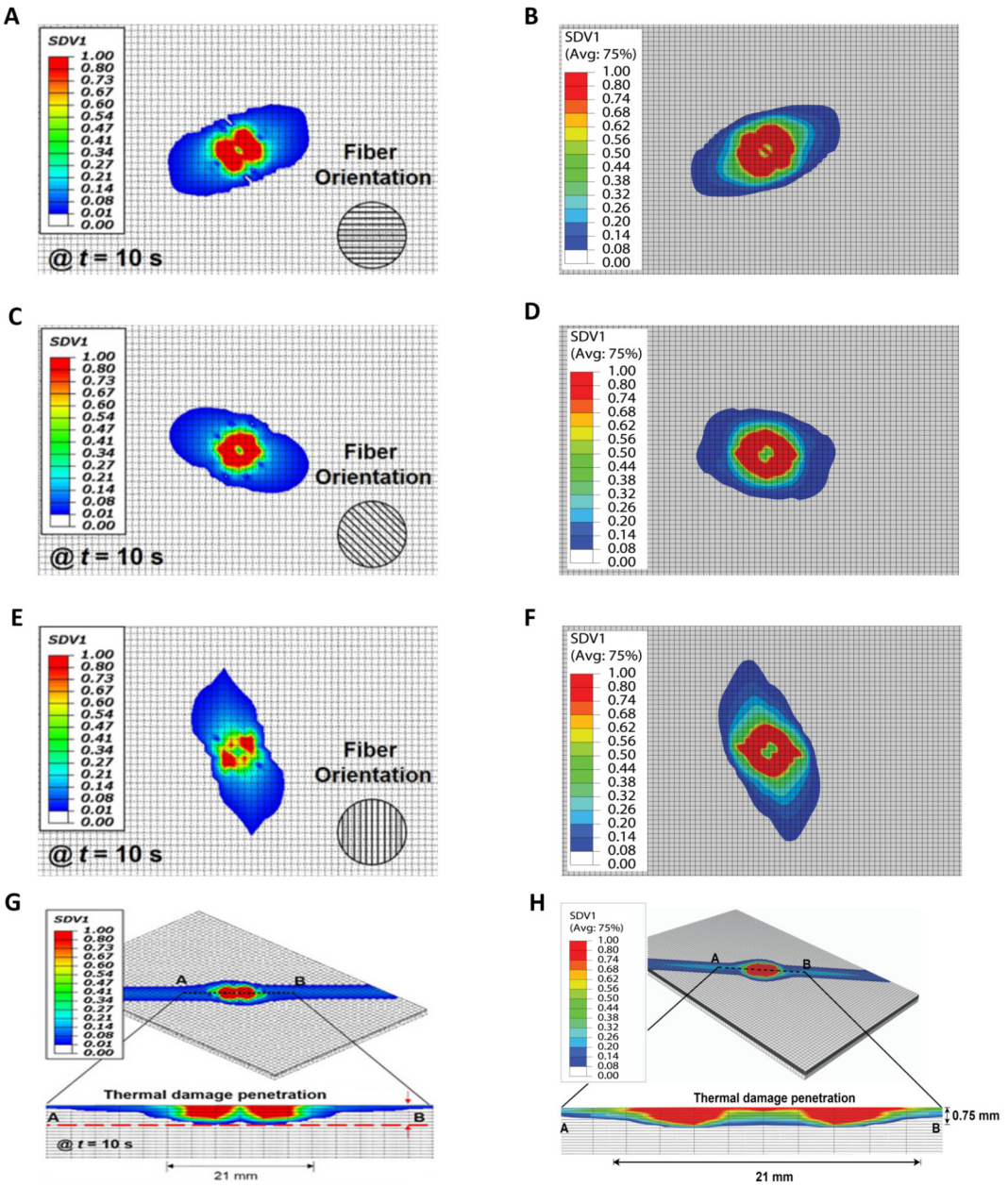

Fig. 4. Comparative results from literature and the current FE model concerning matrix thermal decomposition in 2^{nd}, 3^{rd} and 4^{th} plies and thermal damage penetration in AS4/3506a carbon/epoxy laminate. (A, C, E) Matrix thermal decomposition in 2^{nd}, 3^{rd} and 4^{th} plies respectively predicted by Lee et al. [16] **(B, D, F)** Matrix thermal decomposition in 2^{nd}, 3^{rd} and 4^{th} plies respectively predicted by the current FE model. **(G)** Thermal damage penetration predicted by Lee et al. [16] **(H)** Thermal damage penetration predicted by the current FE model. Note that the results are captured at the end of heat transfer analysis (10 s).

ranges from 300 °C to 500 °C. In Figs. 3(C) and 3(D), thermal damage is defined in terms of SDV1 which is the degree of thermal damage calculated in the HETVAL user subroutine based on the temperature ranging from 300 °C to 500 °C. Hence Fig. 3(B) can be compared with Figs. 3(C) and 3(D) qualitatively. In Fig. 3 (C) and 3 (D), SDV1 is the state variable used in the HETVAL user subroutine which represents the degree of thermal damage. Further, note that Avg. 75% is the 75% threshold value for averaging results in Abaqus cae. To visualize the results in contour plots, the saved results from element integration points need to be extrapolated to element nodes. Averaging computation converts values from the different extrapolated nodal results into a single nodal result. This threshold can be controlled by the user in Abaqus result options. Here the thermal damage was dominant in the nearby areas of the lightning attachment point (i.e. at the center of the laminate). The damage was spread along the fiber direction (i.e., the dominant electrical conduction path) as observed from the physical experiment conducted by Hirano et al. [4]. Fig. 3(E) and Fig. 3(G) show the electrical potential (EPOT) and electrical current density (ECD) distributions respectively in the top composite ply predicted by Lee et al. [16], whereas Fig. 3(F) and Fig. 3(H) show those predicted by the present FE model. The current FE model results are found to be nearly identical to the experimental results of Hirano et al. [4] and FE results of Ogasawara et al. [6] and Lee et al. [16]. Small variations in values obtained from the current analyses and reference literature may be due to solver version issues and other compatibility-related issues. These results essentially establish that the present deterministic FE model is accurate enough for subsequent analyses following a stochastic regime.

We further compare the deterministic results of lightning strike damage in the inner plies. Fig. 4(A, C, E) are the predicted matrix damage in the inner (2^{nd}, 3^{rd} and 4^{th}) plies predicted by Lee et al.

[16] and Fig. 4(B, D, F) are those from the present FE model. For inner plies, the damage domains were found to be more elliptical. The major axis of elliptical-shaped thermal damage is not perfectly aligned along the local fiber direction, indicating somewhat considerable Joule heating occurring through the thickness direction. The domain with intense matrix damage decreases for the successive inner layer. This is reasonable since the amount of current reaching (i.e. correspondingly Joule heating occurring) the underlying plies decreases with depth. Fig. 4(G) is the thermal damage penetration through the laminate thickness predicted by Lee et al. [16] whereas Fig. 4(H) is the thermal damage penetration predicted by the present FE model. In both models, the predicted thermal damage penetration was up to the 6th ply (0.75 mm). Along with the numerical results presented in the preceding paragraph for outer ply, the current results establish that the baseline FE model developed in this study is successfully validated with available experimental observation [4] and quantitative/qualitative numerical analysis of lightning thermal damage characteristics [6,16].

2.3. Quantification of damage through damage severity level

For probabilistic quantification, it is essential to have numerical representation of damage that can correlate with the visual characterization of damage areas. Here the severity of lightning thermal damage is categorized into three damage severity level (DSL) zones based on the degree of damage (SDV1): *i*) DSL-1 representing the minor damage region ($0.4 \leq \text{SDV1} \leq 0.55$), *ii*) DSL-2 representing to the intermediate damage region ($0.55 < \text{SDV1} \leq 0.75$), and *iii*) DSL-3 representing the severe damage region (SDV1 > 0.76). These values are chosen based on engineering judgment and according to the overall range/ distribution of SDV1. The ranges of DSLs can be further adjusted in future studies. Fig. 5(A) presents DSL zones for the top ply of the laminate given for reference purposes. Fig. 5(B) shows the detailed and zoomed view of damaged portions of Fig. 5(A). The predicted domain (outermost ply) from 40kA peak current waveform is 55.5948 mm^2 for the DSL-1 zone, 54.8821 mm^2 for the DSL-2 zone, and 138.0869 mm^2 for the DSL-3 zone. These areas can be used for quantifying the damage severity, along with inclusion of weights if necessary for defining a representative parameter for damage.

In the present context, area of lightning thermal damage is the response parameter. However, there are three different damage severity levels as defined in the preceding paragraph. To have a unified quantifiable measure, we propose weighted damage by assigning appropriate weights corresponding to the areas of damage with different severity level. The parameter of weighted damage for damage severity levels (WDDSL), which allows to assign different importance to each DSL, is calculated as follows:

$$WDDSL = \frac{\sum_{j=1}^{n} \mu_{DSL(j)} A_{DSL(j)}(\omega)}{\sum_{j=1}^{n} A_{DSL(j)}(\omega)} \tag{2}$$

where, n is the number of DSL (i.e., $n = 3$ in this work), $\mu_{DSL(j)}$ is the mean of j^{th} DSL and $A_{DSL(j)}(\omega)$ is stochastic damage area of j^{th} DSL. In a mean sense based on their respective defined bounds, $\mu_{DSL(1)}$, $\mu_{DSL(2)}$, and $\mu_{DSL(3)}$ are taken as 0.45, 0.65, and 0.85, respectively. The values are kept constant for uncertainty analysis in this work for obtaining a consistent understanding in the following sections.

3. Preliminary screening of important parameters for stochastic analysis

In this study, there are nine primary potential input parameters (three orthogonal thermal conductivities, three orthogonal electrical conductivities, specific heat, density, and outermost ply fiber orientation) that can impact the lightning damage of the composite laminate. All the input parameters may not significantly affect the damage of the laminates while a higher number of input parameter would increase the complexity and computational expenses of machine learning model formation. Making all the input parameters stochastic and inclusive of the analysis will increase the number of FE simulations to be performed drastically for analysis. Hence to screen out less important stochastic parameters, a preliminary sensitivity analysis is performed here based on the first-order perturbation theory (FOPT) [36,37] that builds a Taylor series expansion of stochastic variables. A small degree of stochasticity around the mean values of deterministic input parameters ($\boldsymbol{\mu}_{\bar{u}} = \{\mu_{\bar{u}_1}, \mu_{\bar{u}_2}, ..., \mu_{\bar{u}_m}\}$, where $m = 9$) is considered, resulting in stochastic responses $N_0^{Res}(\bar{u})$. The deterministic input parameters used in this work are the experimentally measured material properties, as listed in Table 1. Implementing Taylor series expansion of each stochastic variable, stochastic responses are expressed as

$$N_0^{Res}(\bar{u}) = N_0^{Res}(\boldsymbol{\mu}_{\bar{u}}) + \sum_{i=1}^{m} \left[\frac{\partial N_0^{Res}(\bar{u})}{\partial \bar{u}_i} |_{\bar{u}=\boldsymbol{\mu}_{\bar{u}}} \right] \left(\bar{u}_i - \mu_{\bar{u}_i}\right) + \frac{1}{2} \sum_{i=1}^{m} \sum_{j=1}^{m} \left[\frac{\partial N_0^{Res}(\bar{u})}{\partial \bar{u}_i \partial \bar{u}_j} |_{\bar{u}=\boldsymbol{\mu}_{\bar{u}}} \right] \left(\bar{u}_i - \mu_{\bar{u}_i}\right) \left(\bar{u}_j - \mu_{\bar{u}_j}\right) + \mathbf{H}(\bar{u}) \tag{3}$$

where $\mu_{\bar{u}_i}$ denotes the mean of the i^{th} random input variable, $\mathbf{H}(\bar{u})$ represents higher-order terms of the Taylor series expansion for uncertainty $\bar{u}$. After neglecting the second-order and higher-order terms in the above expression, the mean μ and variance σ^2 of the stochastic responses N_0^{Res} can be estimated as

$$\mu_{N_0^{Res}(\bar{u})} = N_0^{Res}(\boldsymbol{\mu}_{\bar{u}}) \tag{4}$$

$$\sigma^2_{N_0^{Res}(\bar{u})} = \sum_{i=1}^{m} \sum_{j=1}^{m} \left[\frac{\partial N_0^{Res}(\bar{u})}{\partial \bar{u}_i} |_{\bar{u}=\boldsymbol{\mu}_{\bar{u}}} \right] \times \left[\frac{\partial N_0^{Res}(\bar{u})}{\partial \bar{u}_j} |_{\bar{u}=\boldsymbol{\mu}_{\bar{u}}} \right] .cov\left(\bar{u}_i, \bar{u}_j\right) \tag{5}$$

where $cov\left(\bar{u}_i, \bar{u}_j\right)$ is the covariance between the i^{th} and j^{th} input variables, i.e., $cov\left(\bar{u}_i, \bar{u}_j\right) = 0$ if $\bar{u}_i$ and $\bar{u}_j$ are uncorrelated, and $cov\left(\bar{u}_i, \bar{u}_j\right) = \sigma^2_{\bar{u}_i} = \sigma^2_{\bar{u}_j}$ if $i = j$. Assuming negligible correlation among the input variables, the stochastic uncertainty in responses can be obtained using one factor at a time based on the central difference scheme

$$\frac{\partial N_0^{Res}}{\partial \bar{u}_i} = \frac{N_0^{Res}\left(\mu_{\bar{u}_i} + p_i\right) - N_0^{Res}\left(\mu_{\bar{u}_i} - p_i\right)}{2p_i} \tag{6}$$

Here, p_i denotes the perturbation size for i^{th} input variable (the input variables are perturbed here taking ±10% variation around mean deterministic values). After calculating the mean μ and standard deviation σ, the sensitivity of i^{th} input variable ($\tilde{S}_i$) is calculated as

$$\tilde{S}_i = \frac{\left(\frac{\sigma_{N_0^{Res}(\bar{u})}}{\mu_{N_0^{Res}(\bar{u})}} \right)_i}{\sum_{i=1}^{m} \left(\frac{\sigma_{N_0^{Res}(\bar{u})}}{\mu_{N_0^{Res}(\bar{u})}} \right)_i} \tag{7}$$

In the present context, area of lightning thermal damage is the response parameter. However, there are three different damage severity levels as defined in the preceding section. To have a

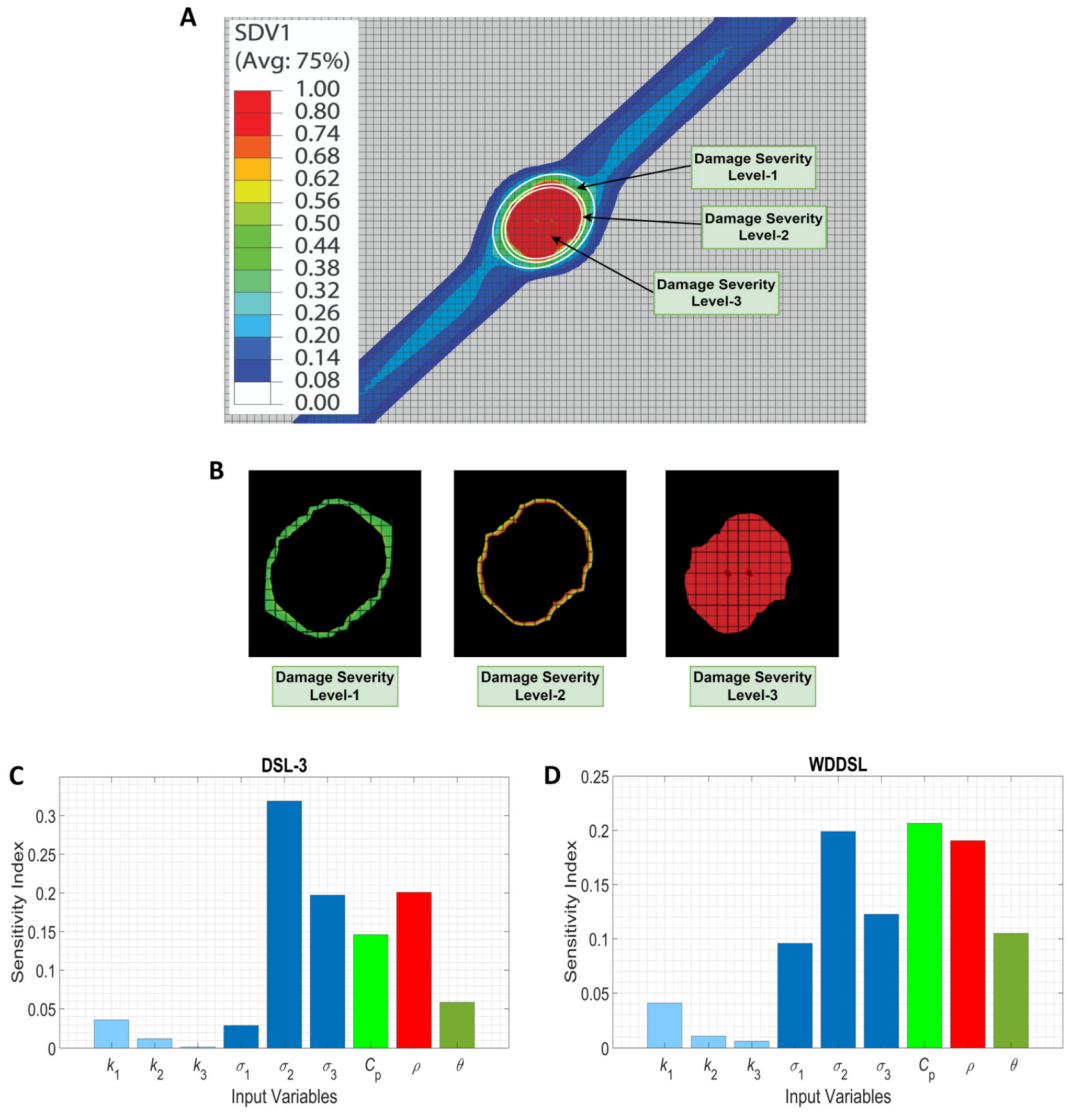

Fig. 5. Definition of damage severity level (DSL) and subsequent preliminary screening of input parameters. (A) DSLs for the top ply of laminate. **(B)** Damaged portions of DSL 1, 2 and 3 in zoomed view. **(C, D)** First-order perturbation theory-based preliminary screening of input parameters considering DSL 3 and WDDSL. Here k_1, k_2, k_3, σ_1, σ_2, σ_3, C_p, ρ, and θ represent thermal conductivities in the longitudinal, transverse, and thickness directions, electrical conductivity in the longitudinal, transverse, and thickness directions, specific heat, density and top ply fiber orientation, respectively. The sensitivity index ($\tilde{S}_i$) is described in section 3.

unified quantifiable measure, we have proposed the concept of WDDSL in this study. The entire set of input parameters involve k_1, k_2, k_3, σ_1, σ_2, σ_3, C_p, ρ, and θ that represent the longitudinal, transverse, through-thickness thermal conductivities, the longitudinal, transverse, through-thickness electrical conductivities, specific heat, density, and top ply orientation, respectively. Through the FOPT based screening approach explained in this section, we would try to identify the most influential input parameters for lightning strike damage. FOPT based sensitivity analysis is performed here for the most severe damage (DSL-3) and weighted damage (WDDSL). Note that the weighted damage includes data from all damage severity levels (DSL-1, DSL-2, DSL-3). Thus, separate sensitivity analysis results for DSL-1 and DSL-2 are not presented.

Fig. 5(C) and Fig. 5(D) present FOPT-based sensitivity analysis of lightning thermal damage in top composite ply based on DSL 3 and weighted damage for damage severity levels (WDDSL), respectively. This figure allows us to screen out insignificant input parameters, the variation of which are not sensitive to the damage areas. This preliminary sensitivity analysis suggests that the thermal conductivities in all orthogonal directions (k_1, k_2, k_3) are the least sensitive to the lightning thermal damage in the laminate. This is consistent with findings from recent studies [18,38]. Hence, thermal conductivities in all orthogonal directions are dropped in the following stochastic analyses. We would construct the machine learning models and carry out subsequent stochastic analysis based on the remaining sensitive input parameters only. In this context, it may be noted that FOPT only gives a preliminary idea of the sensitivity of different input parameters (for preliminary screening purposes) based on a very limited number of FE simulations (three simulations are performed for each input variable, one at mean deterministic value and the other two at perturbed minimum and maximum values). We have presented a comprehensive global sensitivity analysis based on support vector machine based surrogate models later in this study.

4. Support vector machine based stochastic analysis

4.1. Surrogate modeling based on support vector machine

The machine learning model based on Support vector machine (SVM) is exploited here as a computationally efficient mapping between the sets of stochastic input parameter space and uncertain

response quantities of interest [39,40]. SVM regression is a supervised machine learning algorithm where the regression hyperplane is determined by optimizing the distances from the nearest data points, called support vectors [41–45,49,46]. Given that (x_i, v_i) are training data points, $i = 1, 2, 3, ...\tilde{n}$, where $\tilde{n}$ is the number of training data points. The training data is mapped to a high dimensional feature space. After mapping, linear decision function $v(x)$ can be written as

$$v(x) = \mathbf{w}^T x + \alpha \tag{8}$$

where $\mathbf{w}$ is weight vector; α is a bias. The training data which is outside of the ϵ-insensitive tube can be tolerated using slack variables (η_i, η_i^*) [47]. The optimization is done by minimizing the objective function (J) with the constraints

$$J = \frac{1}{2}||\mathbf{w}||^2 + K\sum_{i=1}^{\tilde{n}}(\eta_i + \eta_i^*) \tag{9}$$

subject to

$$\begin{cases} v_i - \mathbf{w}^T x_i - \alpha \leq \epsilon + \eta_i \\ \mathbf{w}^T x_i + \alpha - v_i \leq \epsilon + \eta_i^* \\ \eta_i, \eta_i^* \geq 0 \end{cases}$$

where K is constant regularization parameter and slack variables (η_i, η_i^*) measure the deviation of points which are outside of ϵ. The non-linear regression problem can be solved using Lagrange equation [48] and its solution can be given as

$$v(x) = \sum_{i=1}^{\tilde{n}}(\beta_i - \beta_i^*)C(x_i, x) + \alpha \tag{10}$$

where $(\beta_i - \beta_i^*)$ are Lagrange multipliers and $C(x_i, x)$ is kernel function. Polynomial kernel function is given as

$$C(x_i, x) = (x_i.x + 1)^p \tag{11}$$

where p is the order of the polynomial. The probabilistic responses are predicted at new stochastic data points for uncertainty quantification concerning lightning damage using full scale Monte Carlo simulations [49–51]. Fig. 1(C) shows a schematic representation of the surrogate model-based stochastic analysis adopted here. Probability density function (PDF) of the responses $v(x(\omega))$ (such as DSL, WDDSL, ECD, and EPOT) is shown considering the stochasticity in input parameters $x(\omega)$ (material properties and ply orientation, refer to Fig. 6(B)) where ω denotes the stochasticity of parameters. SVM regression is coupled with Sobol sequence sampling algorithm [29,30,52] in this work for the training and validation of surrogate models.

4.2. Stochastic analysis of lightning thermal damage

Based on the initial sensitivity analysis and studies in available literature [18,38], the thermal conductivities are found to be the least important material properties for lightning thermal damage in composite, and thus ignored in the following stochastic analysis. Instead, we have considered two outermost ply fiber orientations (+45° and 0°) since the extent and shape of lightning thermal damage is strongly influenced by local ply orientation. As consequence, in the following section, a total of seven material properties, including three electrical conductivities (σ_1, σ_2, σ_3), specific heat (C_p), density (ρ), and two outermost ply fiber orientation (+45° and 0°), are considered to study the effect of source-uncertainty on the lightning thermal damage in carbon/epoxy laminate. A random variation of ±10% is taken with respect to the nominal values (as per common industry standards) for all uncertain parameters for performing the stochastic analysis. Monte Carlo (MC) simulation that predicts the response of the system for randomly distributed input variables is adopted in conjunction with support vector machine based surrogates for complete probabilistic quantification. The following stochastic individual and compound cases (denoted as, g^I, g^{II},..., g^V) are considered for performing Monte Carlo simulations in the present study for a comprehensive understanding of the corresponding stochastic effects.

(1) Only randomly-varying electrical conductivities (σ_1, σ_2, σ_3) which can be written as:

$$g^I\{\sigma_1(\omega), \sigma_2(\omega), \sigma_3(\omega)\} = \{\psi^1\left(\sigma_{1(1)}...\sigma_{1(l)}\right), \psi^2\left(\sigma_{2(1)}...\sigma_{2(l)}\right), \psi^3\left(\sigma_{3(1)}...\sigma_{3(l)}\right)\}$$

(2) Only randomly-varying specific heat (C_p) which can be written as:

$$g^{II}\{C_p(\omega)\} = \left\{\psi^1\left(C_{p(1)}...C_{p(l)}\right)\right\}$$

(3) Only randomly-varying density (ρ) which can be written as:

$$g^{III}\{\rho(\omega)\} = \left\{\psi^1\left(\rho_{(1)}...\rho_{(l)}\right)\right\}$$

(4) Only randomly-varying fiber orientations (θ_1, θ_2) which can be written as:

$$g^{IV}\{\theta_1(\omega), \theta_2(\omega)\} = \left\{\psi^1\left(\theta_{1(1)}...\theta_{1(l)}\right), \psi^2\left(\theta_{2(1)}...\theta_{2(l)}\right)\right\}$$

(5) Compound effect of randomly-varying all stochastic input properties (σ_1, σ_2, σ_3, C_p, ρ, θ_1, θ_2) which can be written as:

$$g^V\{\sigma_1(\omega), sigma_2(\omega), \sigma_3(\omega), C_p(\omega), \rho(\omega), \theta_1(\omega), \theta_2(\omega)\} = \left\{\begin{array}{c} \psi^1\left(\sigma_{1(1)}...\sigma_{1(l)}\right), \psi^2\left(\sigma_{2(1)}...\sigma_{2(l)}\right), \psi^3\left(\sigma_{3(1)}...\sigma_{3(l)}\right), \\ \psi^4\left(C_{p(1)}...C_{p(l)}\right), \psi^5\left(\rho_{(1)}...\rho_{(l)}\right), \psi^6\left(\theta_{1(1)}...\theta_{1(l)}\right), \\ \psi^7\left(\theta_{2(1)}...\theta_{2(l)}\right) \end{array}\right\}$$

Operator ψ generates the set of random input parameters for performing MC simulations. $\sigma_{1(i)}$, $\sigma_{2(i)}$, $\sigma_{3(i)}$, $C_{p(i)}$, $\rho_{(i)}$ and $\theta_{1(i)}$, $\theta_{2(i)}$ are material properties and ply orientations respectively, for i^{th} data point. Symbol l denotes the total number of the data point used in MC simulations. We have used ω to represent the stochastic characteristic of the respective parameters.

Fig. 6(A) presents a flow chart of surrogate-based stochastic analysis for uncertainty quantification of lightning thermal damage. The stochastic input variables (i.e., material properties and ply orientation) and corresponding stochastic responses (i.e., DSL, WDDSL, ECD, and EPOT) are shown in Fig. 6(B). In-plane epoxy decomposition in the individual plies of the laminate for a typical random realization of the input parameters is presented in Fig. 6(C-J). The epoxy decomposition contours here are a result of the compound stochastic effect of the involved source uncertainties and these will change from sample to sample. Note that we essentially analyze thousands of such random realization for analyzing the stochastic effects of lightning strike damage in a probabilistic framework.

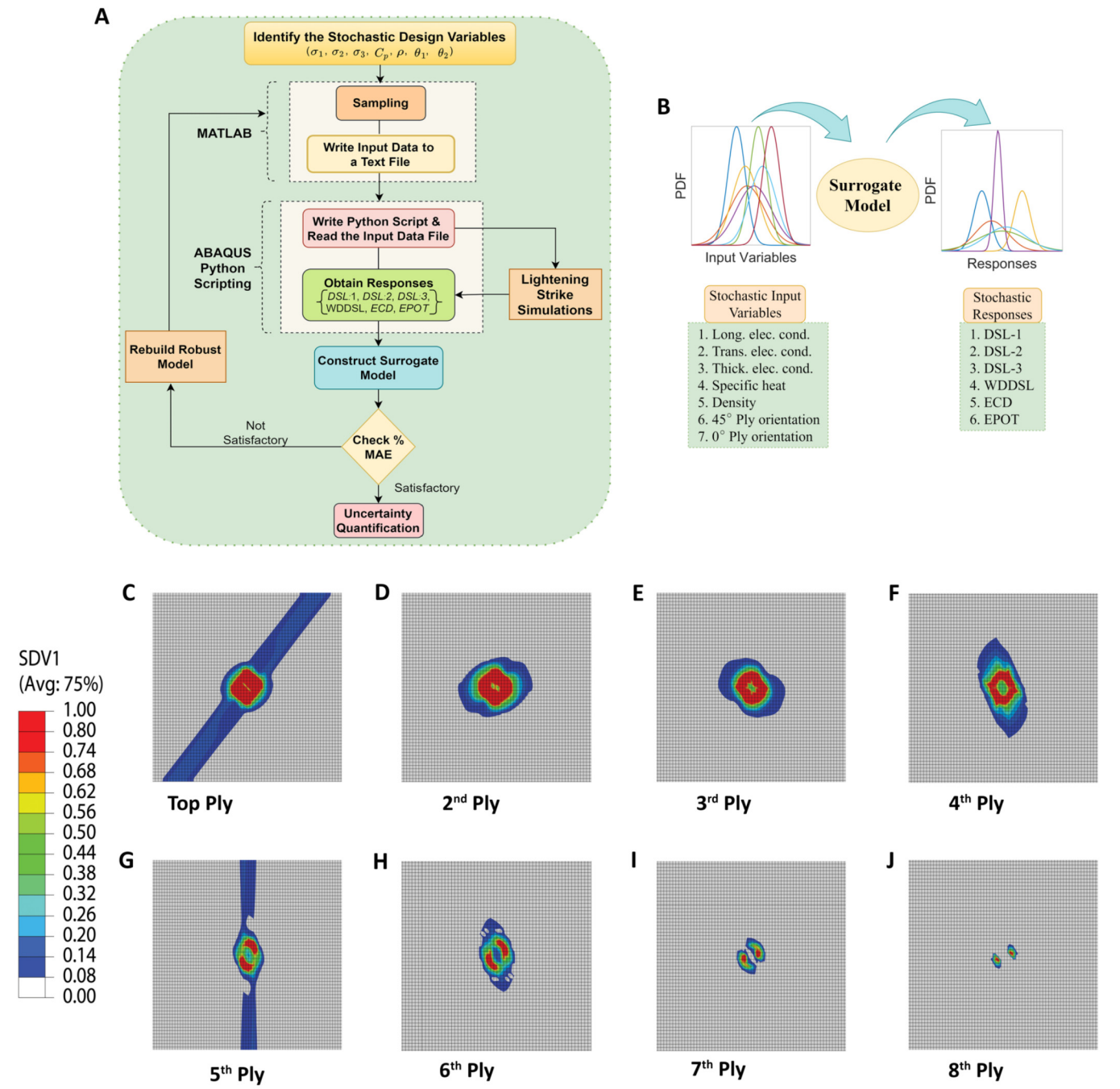

Fig. 6. Description of the computational algorithm for SVM surrogate-based stochastic analysis concerning lightning strike damage. (A) Flow chart of surrogate-based stochastic analysis for uncertainty quantification of in-plane epoxy decomposition in unprotected AS4/3506a carbon/epoxy laminate.**(B)** Stochastic input variables and stochastic outputs of the laminate under lightning strike. **(C-J)** In-plane epoxy decomposition in the individual plies of the laminate for a typical random realization of a set of stochastic input parameters. For a Monte Carlo simulation based stochastic analysis, thousands of such random realizations are analyzed.

4.3. Variance-based global sensitivity analysis

Global sensitivity analysis classifies the relative importance of uncertain input parameters based on the variance of uncertain outputs. First-order sensitivity indices represent the fractional contributions of uncertain inputs in the variance of the output, while total sensitivity indices represent the sum of the main effects of uncertain parameters and all interactions in which those parameters are involved [53]. The algorithm involved in the sensitivity analysis is discussed in the following paragraphs.

Given that N is the number of evaluations, we obtain two (N, k) matrices called P and Q using the Latin hypercube sampling method for the k dimensional model. We define a matrix R_i, which has all columns of the matrix Q except i^{th} column that has been taken from matrix P. Taking input from P, Q and R_i matrices, three outputs $(N, 1)$ are written as

$$\tilde{y}_P = f(P), \qquad \tilde{y}_Q = f(Q), \qquad \tilde{y}_{R_i} = f(R_i) \tag{12}$$

The first-order indices are calculated as [54]

$$S_i = \frac{Var\left[E\left(Y|X_i\right)\right]}{Var\left(Y\right)} = \frac{\tilde{y}_P.\tilde{y}_{R_i} - \bar{f}^2}{\tilde{y}_P.\tilde{y}_P - \bar{f}^2} = \frac{(1/N)\sum_{j=1}^{N} \tilde{y}_P^{(j)} \tilde{y}_{R_i}^{(j)} - \bar{f}^2}{(1/N)\sum_{j=1}^{N} \left(\tilde{y}_P^{(j)}\right)^2 - \bar{f}^2} \tag{13}$$

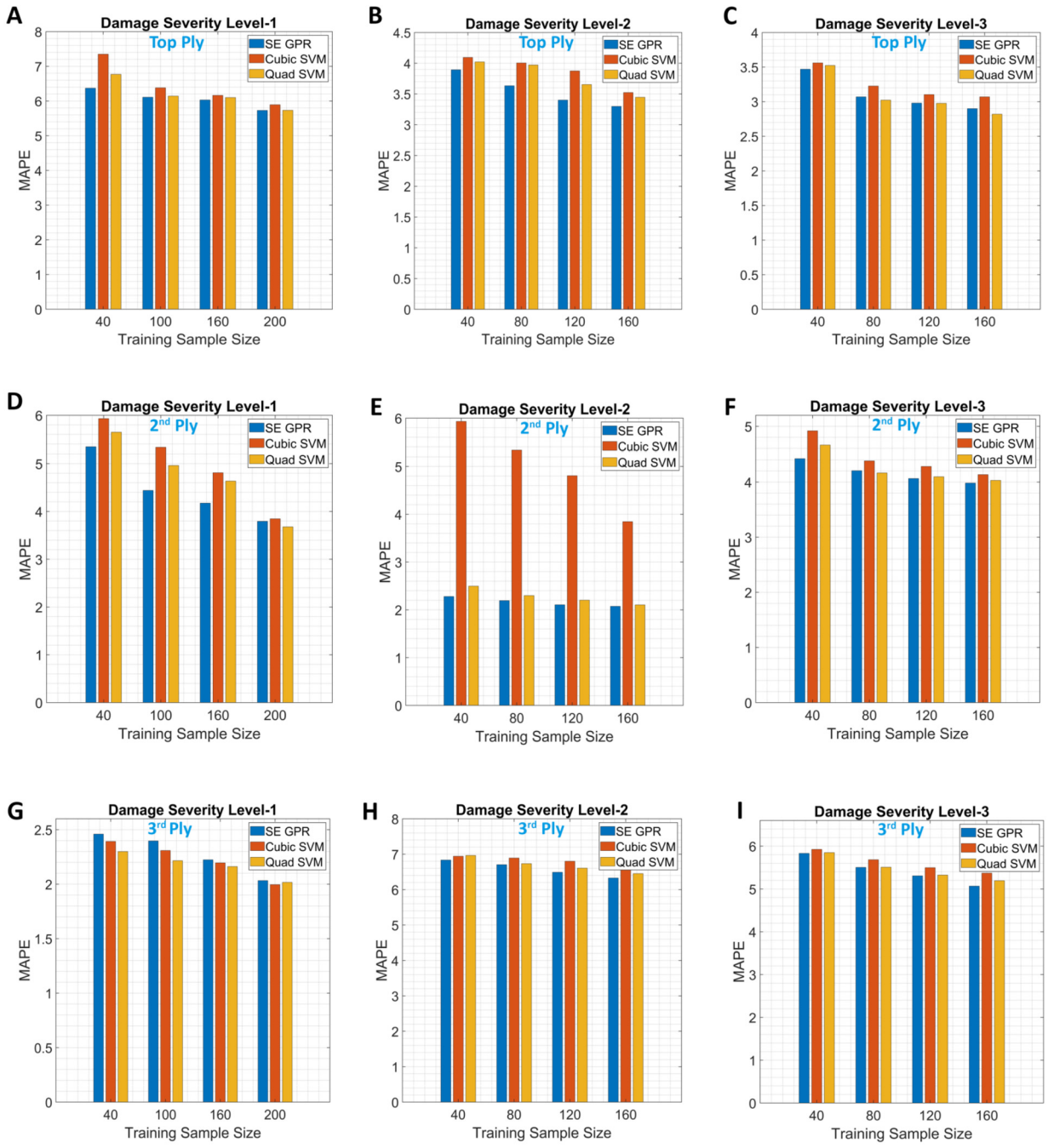

Fig. 7. Mean absolute percentage error (MAPE) of DSLs obtained from squared exponential Gaussian process regression (SE-GPR), and cubic and quadratic SVM regression models considering various training sample sizes. (A, B, C) Top ply. **(D, E, F)** 2^{nd} ply. **(G, H, I)** 3^{rd} ply.

where

$$\bar{f}^2 = \left(\frac{1}{N} \sum_{j=1}^{N} \tilde{y}_P^{(j)} \right)^2$$

The total effects are calculated as

$$S_i^T = 1 - \frac{Var\left[E\left(Y|\mathbf{X}_{\sim i}\right)\right]}{Var\left(Y\right)} = 1 - \frac{\tilde{y}_P . \tilde{y}_{R_i} - \bar{f}^2}{\tilde{y}_R . \tilde{y}_P - \bar{f}^2}$$
$$= 1 - \frac{(1/N)\sum_{j=1}^{N} \tilde{y}_P^{(j)} \tilde{y}_{R_i}^{(j)} - \bar{f}^2}{(1/N)\sum_{j=1}^{N} \left(\tilde{y}_P^{(j)}\right)^2 - \bar{f}^2} \quad (14)$$

The notation $\mathbf{X}_{\sim i}$ denotes the set of all variables except $\mathbf{X}_i$. The simplest way of computing sensitivity indices is by brute force, which is computationally intensive. N^2 number of evaluations are required in brute force method. The number of evaluations in the given method is less than the brute force method. Matrix P, Q, and R_i, in total, give $N(k+2)$ points in the input space; hence a total of $N(k+2)$ runs are required to calculate the sensitivity indices. If we take the sample size as 10000 (i.e. $N = 10000$) for a 7-dimensional model (i.e. $k = 7$) then in the brute force method, 10^8 number of runs are required, whereas the present method will require only 90000 runs to evaluate the sensitivity indices.

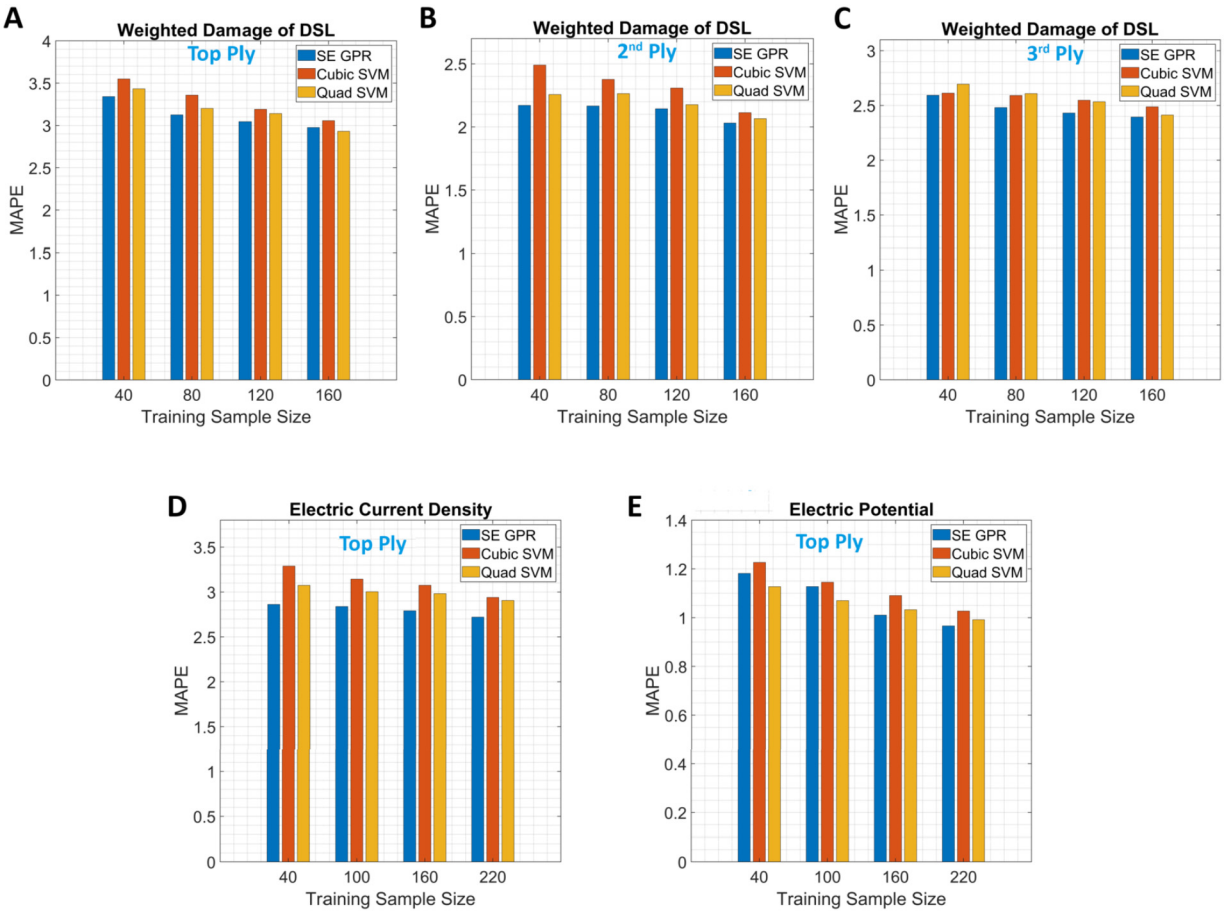

Fig. 8. Mean absolute percentage error (MAPE) as a function of training sample size for WDDSL, ECD and EPOT. (A, B, C) MAPE for WDDSL of top, 2^{nd} and 3^{rd} plies. **(D)** MAPE for electrical current density (ECD). **(E)** MAPE for electrical potential (EPOT). Here responses ECD and EPOT are considered for the maximum values in each sample's top ply of the laminate.

5. Uncertainty quantification and global sensitivity analysis of lightning strike damage

5.1. SVM-based surrogate model validation

The validation of the baseline (deterministic) FE model is already presented in Section 2.2. This section discusses the details on the prediction accuracy of SVM based surrogate models. After having adequate confidence based on such validation (involving both the deterministic FE model and the prediction capability of the machine learning models), we have carried out uncertainty quantification and global sensitivity analysis by exploiting the efficient surrogates of the baseline lightning damage model (refer to Figs. 3 and 4). As discussed previously, the simulated composite considered in this work is a AS4/3506 carbon/epoxy laminate $[45/0/-45/90]_{4S}$ under the effect of a modified component D waveform (40 kA peak amplitude). The stochastic variation in the material properties and ply orientation are taken to quantify the uncertainty in in-plane epoxy matrix thermal decomposition (indicative of lightning thermal damage) and electrical responses of the laminate. Training samples are generated from an optimal Sobol sequence algorithm [29]. Abaqus/standard 2016 version with the following computer specification is used to run FEA simulations: Intel(R) Xeon(R) W-1290 CPU at 3.20 GHz processor speed and 64 GB RAM, wherein 8 cores are utilized in parallel computing for surrogate model construction. The accuracy of surrogate models is investigated by considering different sample sizes for deciding the converged number of training sample data. For quantifying the prediction accuracy of surrogates, mean absolute percentage error (MAPE) is calculated as follows

$$MAPE = \frac{1}{\tilde{N}} \sum_{p=1}^{\tilde{N}} \frac{ABS(Actual_p - Predicted_p).100\%}{Predicted_p} \tag{15}$$

where $\tilde{N}$ is number of samples used for prediction, ABS is absolute of the percentage error, $Actual_p$ is actual response from finite element simulations, $Predicted_p$ is prediction of the surrogate model (for p-th realization).

Fig. 7 presents the mean absolute percentage error (MAPE) of each DSL in the 1^{st}, 2^{nd}, and 3^{rd} carbon/epoxy plies, respectively, plotted for various training sample sizes $\tilde{N}$. Similar MAPE plots are generated for WDDSL, ECD, and EPOT in Fig. 8. In theses figures, each group of bar plots represents the prediction of three different surrogates, while the results are presented for different sample sizes. Surrogate model accuracy depends on the type of supervised machine learning algorithm along with the training sample size, size of input parameter space, degree of complexity involved in the actual simulation model (i.e. the finite element model in the current analysis) and other surrogate tuning parameters. As per earlier studies concerning composites [23], three best-performing machine learning algorithms are shown for comparison in prediction capability including two SVM regression models (cubic and quadratic) and Gaussian process regression (GPR) with squared exponential (SE) kernel. GPR is a nonparametric probabilistic regression method based on Bayesian statistics, the further detail of

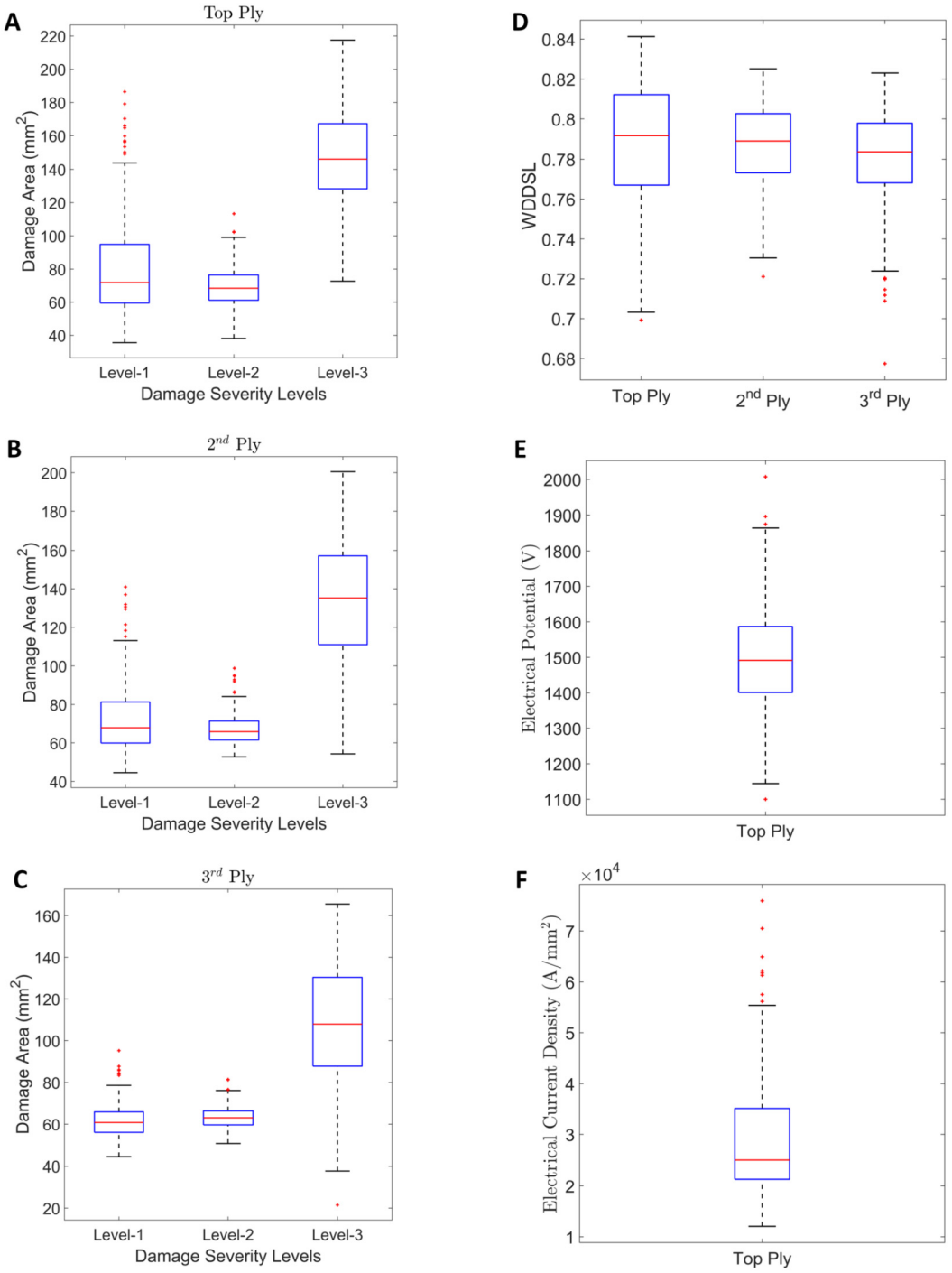

Fig. 9. Box plots of DSLs, WDDSL, EPOT, and ECD. (A, B, C) DSLs for the top, 2^{nd}, and 3^{rd} plies. **(D)** WDDSL for the 1^{st}, 2^{nd} and 3^{rd} plies. **(E)** Maximum value of EPOT for top ply. **(F)** Maximum value of ECD for top ply.

which can be found in literature [28,55]. In Fig. 7, MAPE estimated by GPR and two SVM regression models are compared for each DSL in the top three carbon/epoxy plies. The MAPE decreases (indicating better prediction) with increasing training sample size, wherein we try to identify an optimal size of the training samples that provide adequate accuracy. Based on the presented results, the sample size is chosen as 200 for DSL-1, 160 for DSL-2, DSL-3 and WDDSL, while 220 for ECD and EPOT. Note that, along with the consideration of avoiding overfitting, we have tried to identify the optimal sample size for each of the response parameters as the computational time increases for the surrogate model formation in case of more training data. The prediction performance of Quad SVM and SE GPR are quite comparable. In this context, the prediction accuracy of Cubic and Quad SVM reveals interesting insights. Cubic SVM is a SVM based surrogate trained using cubic polynomial kernels. It is a higher-order polynomial kernel and may require more training data for obtaining adequate prediction accuracy depending on the nature of the underlying physics of the system. In such situations, lower-order kernels (such as quadratic) may obtain better prediction accuracy for a lower sample size [56–59]. However, the higher-order kernels would provide better accuracy when more training data is available. Keeping the constraint of sample size (due to computational expenses) and the required level of accuracy in mind, one needs to select the order of polynomial kernel

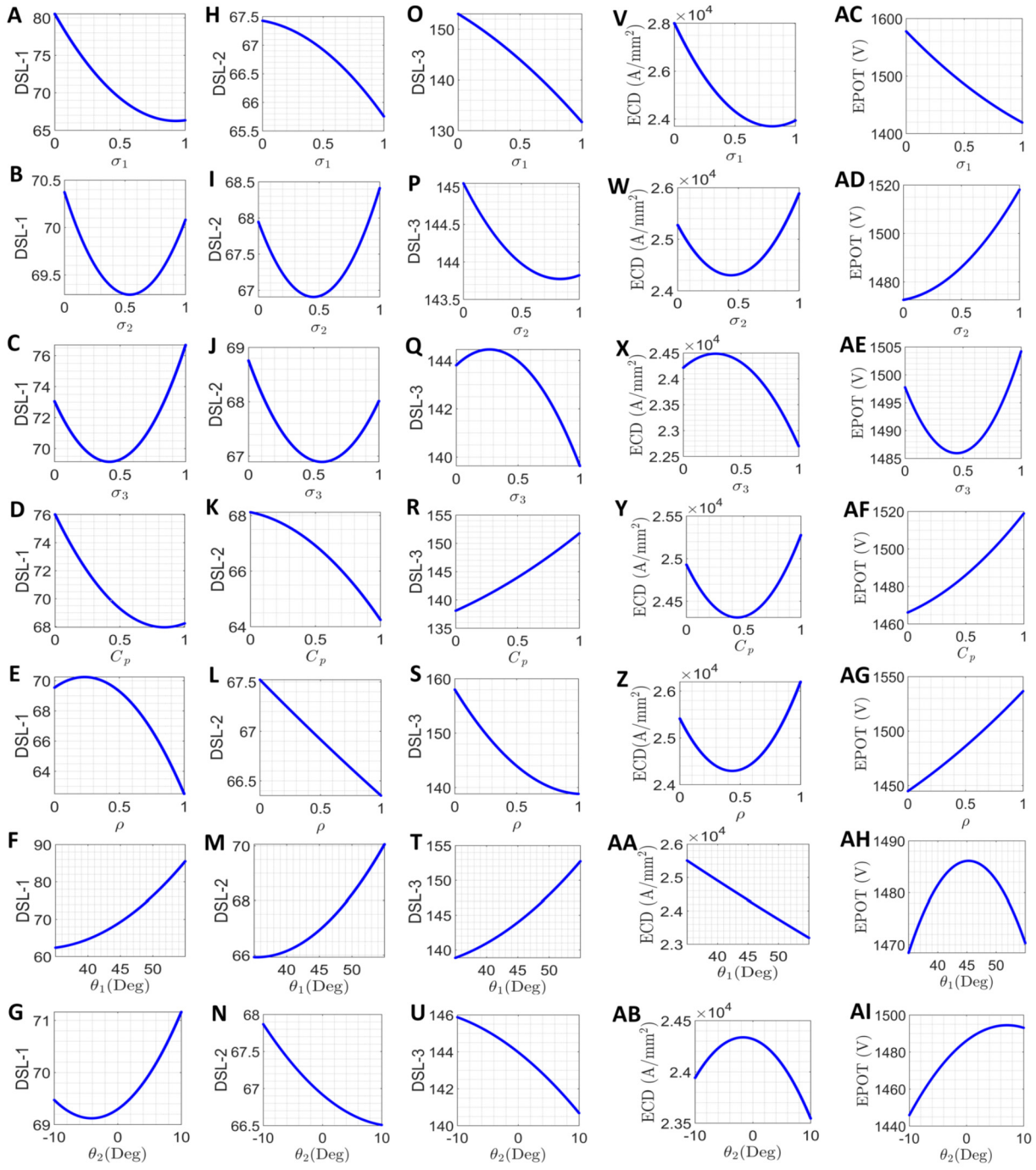

Fig. 10. Effect of deterministic individual variation in the critical input parameters on DSLs, ECD, and EPOT in the top ply of the laminate. (A-G), (H-N), (O-U), (V-AB), (AC-AI) Influence of deterministic variation in input parameters on DSL-1, DSL-2, DSL-3, ECD, and EPOT, respectively in the top ply of the laminate. Here, σ_1, σ_2, σ_3, C_p, ρ, θ_1, and θ_2 represent electrical conductivities in the longitudinal, transverse, and thickness directions, specific heat, density, and +45° and 0° outer layers' ply orientations. In all the presented subplots, 10000 data points are taken along x axis and corresponding y values are obtained using ML model. Since we have used ML model here, it is possible to perform the analysis quite efficiently without using actual expensive FE simulations directly.

through appropriate engineering judgment. In general, SVM based regression methods are robust to outliers in the data, as the decision boundary is determined by the support vectors. This feature of SVMs gives an advantage in the current work as the output data has some outliers here (refer to Fig. 9). In the subsequent section, we present the uncertainty quantification and sensitivity analysis based on Quad SVM considering the training sample sizes discussed above. Here, for all the response parameters corresponding to the chosen optimized training sample sizes, the low values of MAPE (below 2 to 7%) ensure the accurate prediction ability of the surrogates for further analyses.

5.2. Results and discussion

5.2.1. SVM-assisted prediction and uncertainty quantification

In this section, we first present a critical deterministic analysis on the effect of the influencing parameters on the multi-physical responses concerning lightning strike and a statistical analysis of the related physics-based data. Subsequently, complete probabilis-

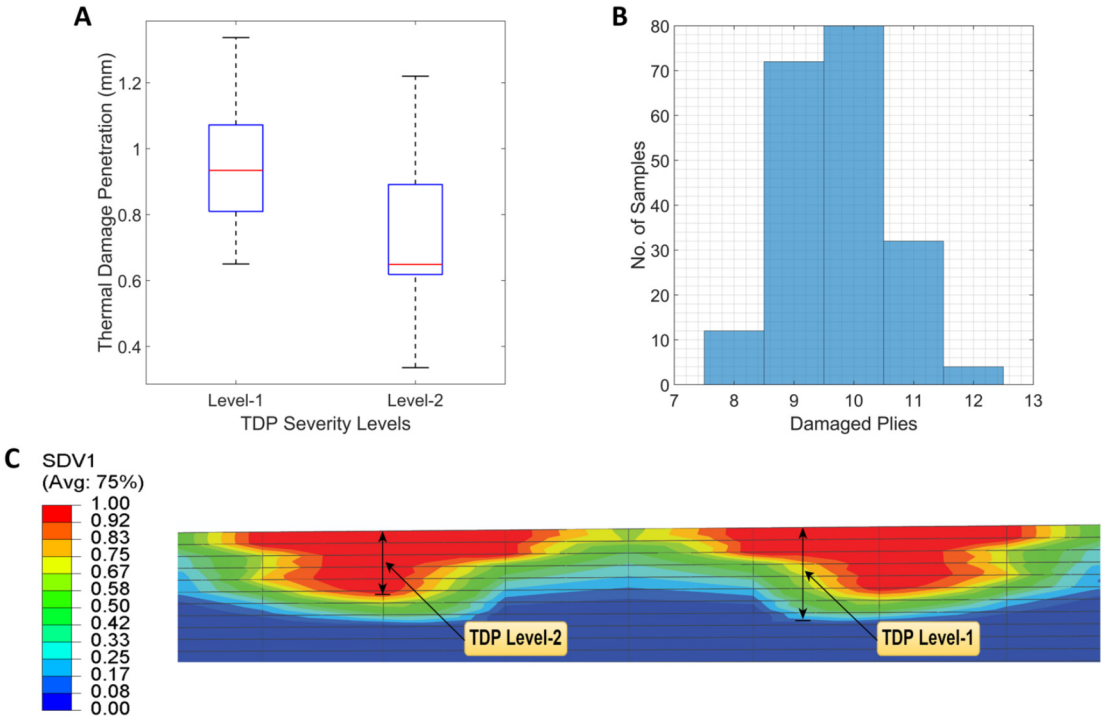

Fig. 11. Through-thickness analysis of stochastic thermal damage penetration (TDP). (A) Box plot of thermal damage penetration (TDP) severity levels. **(B)** Histogram of the number of damaged plies for a stochastic simulation. **(C)** Typical representation of thermal damage penetration (TDP) showing the depths of different damage severity levels for a random realization of set of input parameters.

tic characterization and global sensitivity analysis are presented. Fig. 9 shows the box plots of the lightning thermal damage in the top three outer plies, WDDSL, EPOT, and ECD, respectively. It can be observed that the median of thermal damage area (the horizontal red line in the box) for the DSL-3 reduces from 146.1479 mm^2 in the top ply to 107.9253 mm^2 in the 3^{rd} ply. Similarly, the damaged area in the inner plies reduces for DSL-1 and DSL-2. This makes sense physically since lightning thermal damage in successive carbon/epoxy plies gradually decreases. The box plot for WDDSL (Fig. 9(D)) shows a comparable median with the DSLs (since WDDSL is the weighted average of all DSLs), decreasing slightly for the inner plies. The box plots of ECD and EPOT are presented in Figs. 9(E) and 9(F). Here ECD and EPOT values are found to be maximum in the top ply of the laminate. However, it can be noted that the maximum values of ECD and EPOT remain mostly unchanged till 3^{rd} ply from the top of the laminate since electrical conduction occurs much faster than heat conduction. Hence results are shown here only for the top ply. ECD value varies from 12059.1162 A/mm^2 to 75939.23 A/mm^2 with a median of 24960.33 A/mm^2 whereas EPOT value varies from 1100.2 V to 2007.43 V with a median of 1491.6037 V.

The variations in deterministic DSLs, EPOT, and ECD in the top ply of the laminate concerning influencing input parameters are investigated through the SVM-based surrogate model, as presented in Fig. 10. We follow a one-at-a-time (OAT) method here and it shows how each input variable, throughout their design bounds, influences the thermal and electrical responses of the laminate without considering any correlation. Fig. 10(A, H, O) shows that lightning damage reduces with an increase in the electrical conductivity in the longitudinal direction (σ_1) and density (ρ). The maximum values of ECD and EPOT in the top ply also reduce with an increase in σ_1 (refer to Fig. 10(V, AC)). Fig. 10(F, M, T) shows that the thermal damage increases with an increase in ply orientation angle (top ply). However, Fig. 10(N, U) shows that DSL-2 and DSL-3 decrease with an increase in ply orientation angle of the second ply. Interestingly, we notice maxima and minima of DSLs, ECD and EPOT corresponding to multiple influencing input parameters (such as Figs. 10(B-E, G, I, J, P, Q, V-Z, AB, AE, AH, AI)). Such a thorough understanding of the multiphysical responses would have significant implications for optimum designs.

It can be noted that DSL or WDDSL are defined here for characterizing in-plane lightning thermal damage. It is also critically important to investigate the through-thickness damage propagation to quantify the extent of lightning strike effect. To address this, a new parameter called thermal damage penetration (TDP) is introduced here. It is defined by the maximum damage penetration depth corresponding to different damage severity levels, as explained in Fig. 11(C) for a random realization. Based on the stochastic simulations, it is noted from Fig. 11(A) that TDP level-1 ranges from 0.65 mm to 1.3369 mm whereas TDP level-2 ranges from 0.33549 mm to 1.2198 mm. The histogram presented in Fig. 11(B) considers TDP of top plies which are severely affected as well as the bottom plies which are less affected by the damage. It is noted that 10 plies are damaged in most of the realizations, while it may range up to 12 plies depending on the compound influence of stochastic parameters. A combined understanding of ply-wise DSL, WDDSL and TDP can reflect the extent of lightning strike damage comprehensively. As we notice that the area of lightning damage corresponding to different DSL reduces significantly after first few plies from the top, we only concentrate on the first three layers in the subsequent probabilistic analysis for presenting numerical results.

The complete probabilistic descriptions for ECD, EPOT, DSLs, and WDDSLs are presented in Figs. 12 to 14 based on Monte Carlo simulation considering large-scale realizations ($\sim 10^4$) taking the individual and combined effect of stochasticity in the temperature-dependent material properties and fiber orientation angles. Fig. 12 shows that the longitudinal electrical conductivity (Electrical Cond 1 in the label) has the highest stochastic bounds, which means that this parameter is most sensitive to ECD and EPOT of the laminate.

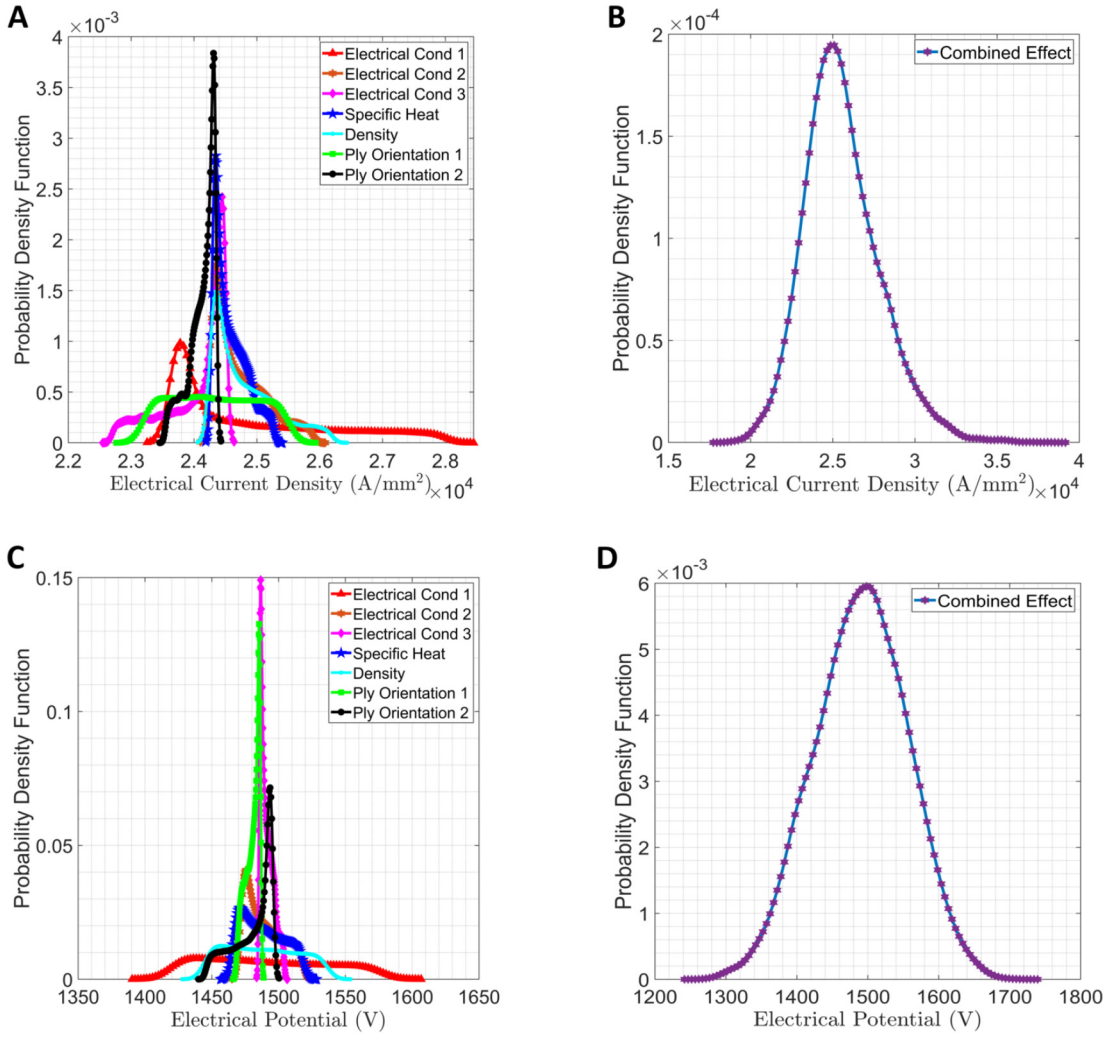

Fig. 12. Probability density function (PDF) plots for electrical current density (ECD) and electrical potential (EPOT). (A, B) PDFs of ECD representing individual and compound stochastic effects of the input variables. **(C, D)** PDFs of EPOT showing individual and compound stochastic effects of the input variables (refer to section 4.2 for individual and combined stochastic effects). The input variables are electrical conductivity in the longitudinal (1), transverse (2), and thickness (3) directions, specific heat, density, and the +45° and 0° ply orientations (denoted by 1 and 2 in the label).

This is consistent with the experimental observation [1] and our earlier study [60]. As shown in Fig. 13, top ply orientation (Ply orientation in the label), specific heat and electrical conductivity in the longitudinal direction have the highest stochastic bounds for all DSLs in the top composite ply. Although not included in the figure, the PDFs generated for DSLs in the 2^{nd} and 3^{rd} ply are also found to be consistent with Fig. 13.

Probabilistic descriptions of WDDSLs for the top, 2^{nd} and 3^{rd} composite plies are presented in Fig. 14, wherein it can be observed that the stochastic output bounds and probabilistic distribution depend strongly on the nature of the source uncertainty under consideration. The combined effect of all the uncertain input variables leads to the highest stochastic response bounds for all the output quantities of interest (refer to section 4.2 for combined stochastic effect). We notice that the stochastic bounds of different individual stochastic parameters follow the order of corresponding sensitivity for all the output quantities of interest. Interestingly, eventhough the probabilistic descriptions of individual stochasticity cases are non-gaussian, the compound stochastic effects become more Gaussian in nature probabilistically. Such observation is consistent with the central limit theorem of probability theory.

5.2.2. Global sensitivity analysis

A variance-based global sensitivity analysis [54] is presented here. The global sensitivity analysis indices (Refer to section 4.3) are found to converge at $\sim 10^4$ samples. The lightning strike electrical charge transfer is a measure of the amount of the electrical energy dissipated by current flowing through a material, which is the product of the ECD vector and the electric field intensity (equivalent to EPOT gradient) vector [16]. Hence, a global sensitivity analysis is performed to evaluate the importance of each stochastic input parameter for ECD and EPOT distributions, as shown in Fig. 15. As stated previously, σ_1, σ_2, σ_3, C_p, ρ, θ_1, and θ_2 in the figure label denote electrical conductivities in the longitudinal, transverse, and thickness directions, specific heat, density, and ply orientations of +45° and 0°, respectively. From the global sensitivity analysis for ECD and EPOT, σ_1 is found to be the most sensitive parameter, i.e., a small variance in σ_1 can lead to a significant change in electrical behavior of the composite subjected to lightning strike. This makes sense since electrical current flow primarily depends on the optimal conduction path (i.e., in the fiber direction). In turn, the sensitivity of DSL and WDDSL would depend on such outcomes and can be correlated to the sensitivity of ECD and EPOT.

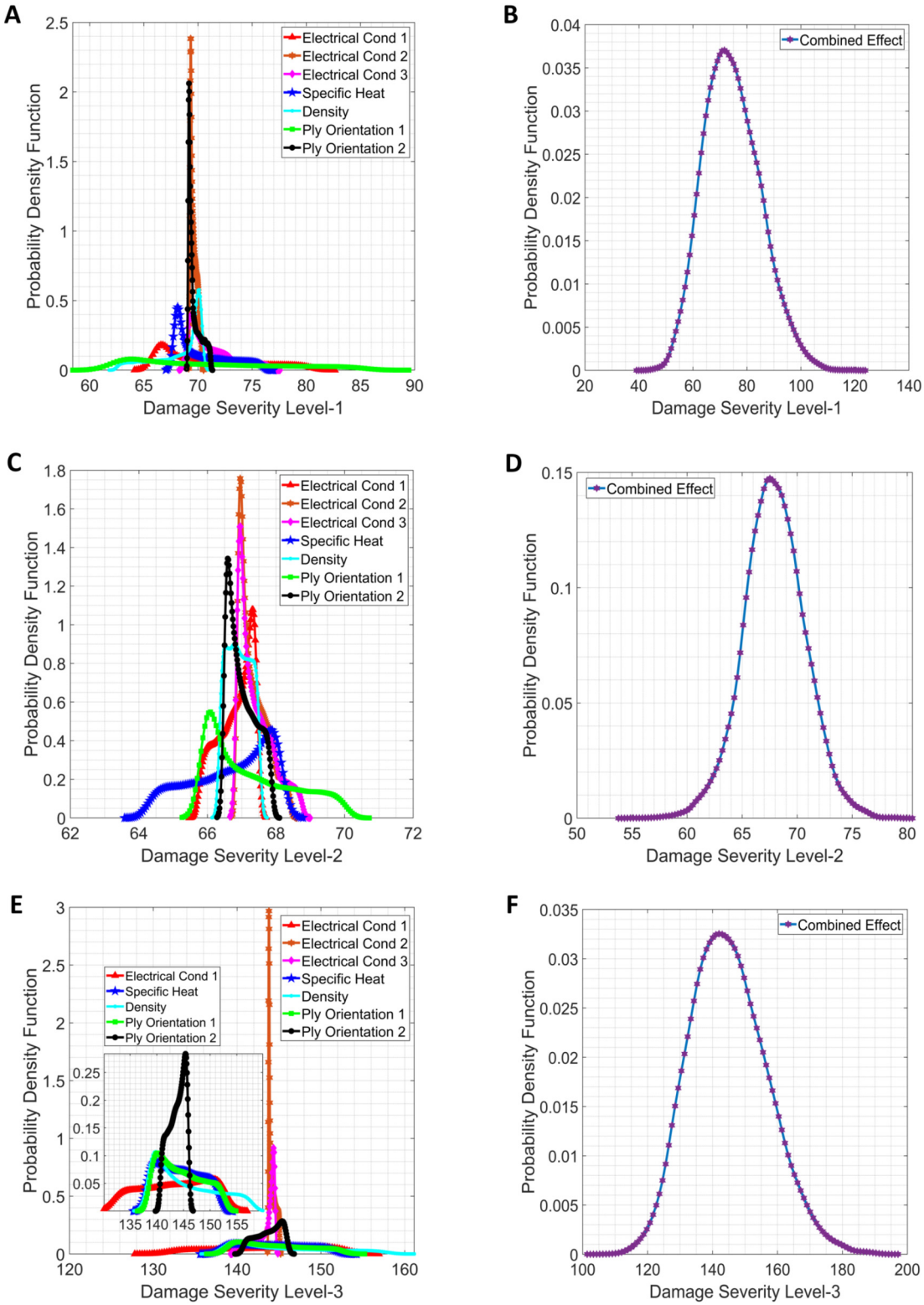

Fig. 13. Probability density function (PDF) plots for each DSL of the top ply. (A, C, E) PDFs for DSL-1, DSL-2 and DSL-3 taking individual stochastic effects of input variables. **(B, D, F)** Corresponding PDFs having compound stochastic effects of the input variables.

Fig. 16 shows the global sensitivity analysis results performed for DSLs and WDDSL of the top ply of the laminate. Considering different output quantities of interest, for DSL-1 (i.e., the minor damage region), θ_1, σ_1, and C_p are the most sensitive (in descending order of sensitivity) parameters, while σ_2, σ_3, ρ, and θ_2 are least sensitive input parameters. In addition, for DSL-2 (i.e., the intermediate damage region), C_p, θ_1, ρ, σ_1, and σ_3 are the most sensitive parameters. In contrast to DSL-1 and DSL-2, the global sensitivity analysis result for DSL-3 shows that σ_1, ρ, C_p, and θ_1 are the most sensitive parameters. This result shows good agreement with the existing experimental and numerical studies. However, it becomes evident that the relative sensitivity of differ-

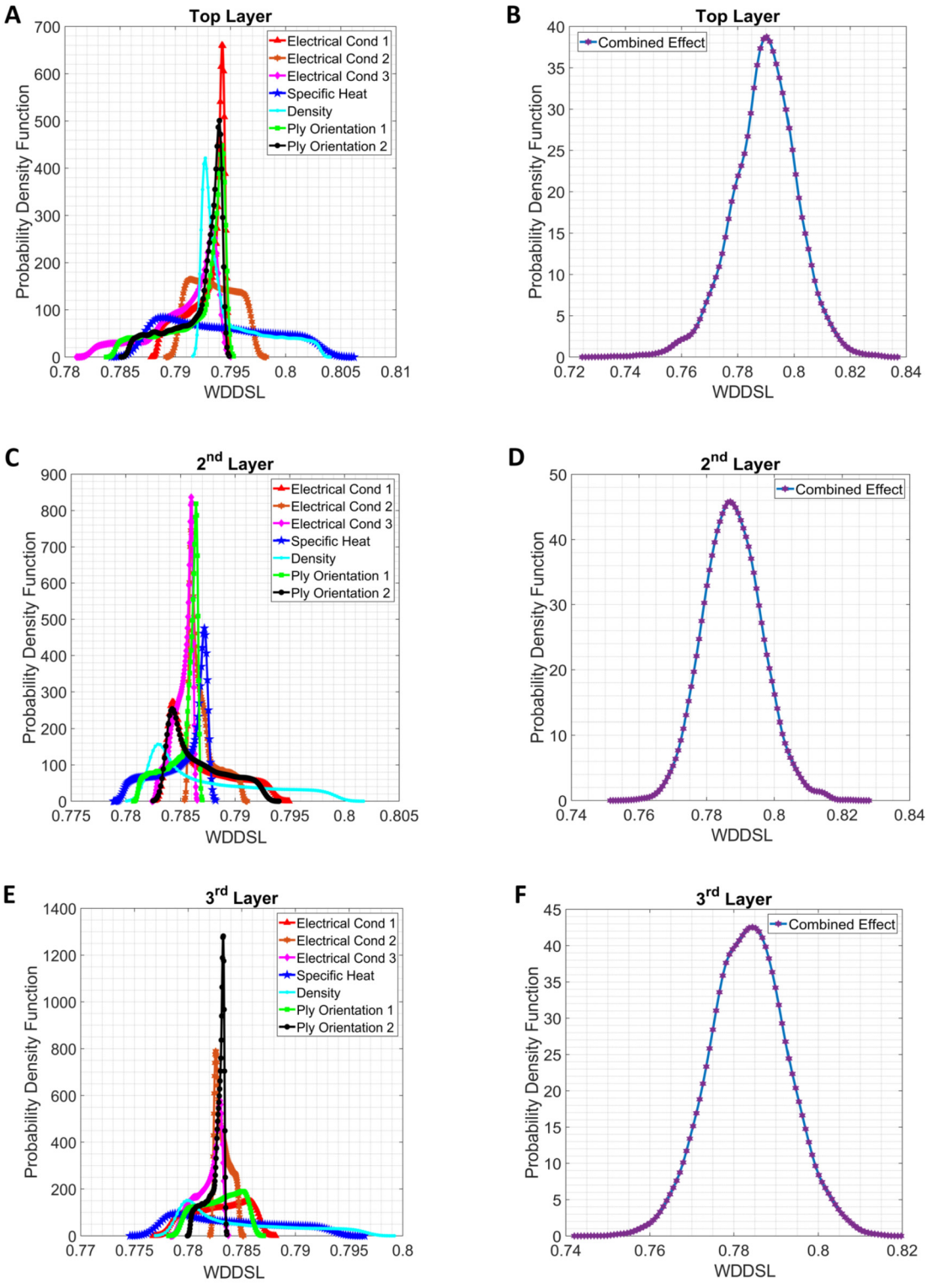

Fig. 14. Probability density function (PDF) plots for WDDSL of the top, 2^{nd} and 3^{rd} plies. (A, C, E) PDFs for WDDSL of the top, 2^{nd} and 3^{rd} plies respectively taking individual stochastic effects of input variables. **(B, D, F)** Corresponding PDFs having compound stochastic effects of the input variables.

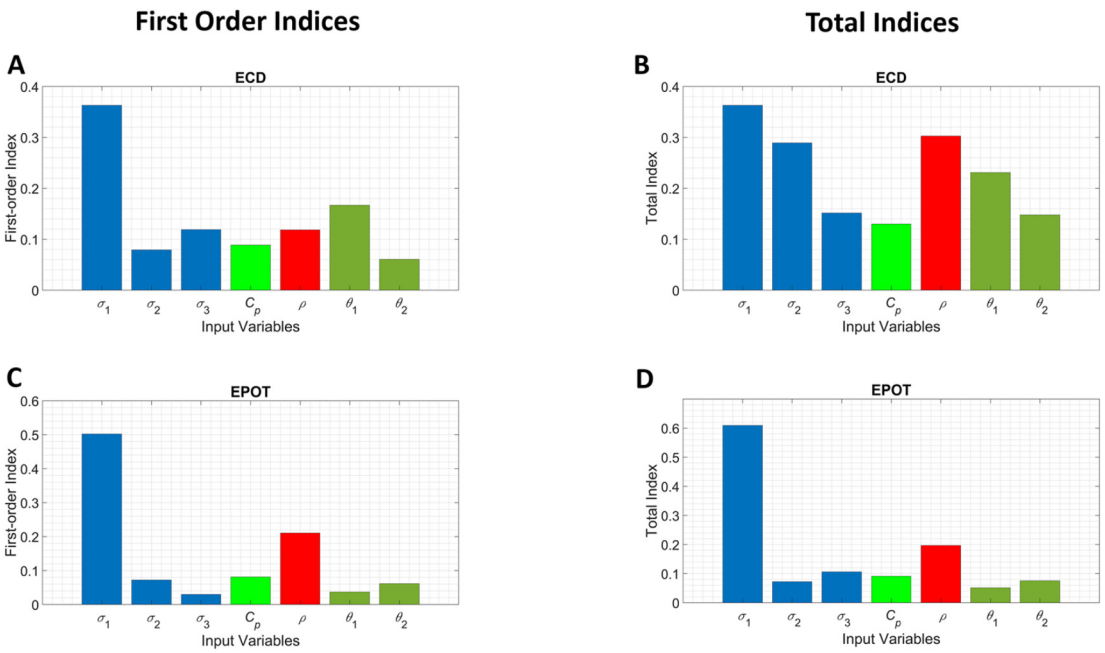

Fig. 15. Variance-based global sensitivity analysis for ECD and EPOT to understand the relative importance of the uncertain input parameters. (A, B) 1^{st} order and total sensitivity indices for ECD. **(C, D)** 1^{st} order and total sensitivity indices for EPOT.

ent influencing input parameters depend on the damage sensitivity level, which has not received attention so far from the scientific community. Although there is little work on varying ρ, C_p, and θ_1 on lightning damage assessment, it is well accepted that lightning thermal damage in carbon/epoxy composite strongly depends on its σ_1. Interestingly, the global sensitivity analysis result for WDDSL shows that C_p is the most significant material property followed by the other parameters due to the incorporation of weights in the definition of WDDSL. This makes sense since C_p is the heat capacity divided by the weight of a material, indicating a measure of the material's heat storage ability. In general, while the results for first order and total sensitivity analysis are consistent to identify the most sensitive input parameter (both of these indices are presented here for giving a comparative perspective), the total sensitivity can be regarded as a more accurate measure.

6. Conclusions and perspective

This paper presents an efficient support vector machine based surrogate approach coupled with computationally intensive transient thermal-electrical finite element simulations to quantify the uncertainty in lightning strike damage of carbon-epoxy composites. The uncertainty in epoxy matrix damage and electrical responses of unprotected carbon/epoxy composite laminates is probabilistically quantified considering the stochasticity in temperature-dependent multi-physical material properties and ply orientations. Such source-uncertainties can be regarded as the consequence of inevitable random variabilities in manufacturing complex material and structural systems like laminated composites, service-life degradations and operational variabilities in extreme environments. For quantifying damage we have proposed the concepts of damage severity levels (DSL) and their weighted variants (WDDSL) along with thermal damage penetration (TDP) for through-thickness damage. The source uncertainty in temperature-dependent material properties (i.e., electrical conductivities, specific heat, density) and geometric attributes like ply orientation angle is propagated here from the input level to the global response level of lightning strike damage characteristics through Monte Carlo simulations. Due to the adoption of a coupled support vector machine based simulation approach in the bottom-up uncertainty propagation framework, it has become possible to carry out a comprehensive uncertainty quantification leading to complete probabilistic descriptions of the electrical and damage parameters despite the requirement of performing a large number of computationally intensive function evaluations. Further, the surrogate models are exploited for an efficient variance-based global sensitivity analysis to investigate the input parameters' relative influence on the lightning strike-induced damage behavior. The results reveal that source-uncertainty of the unprotected laminates significantly influences the epoxy decomposition, electrical current density and electric potential, wherein longitudinal electrical conductivity is most sensitive to stochastic variations followed by other electrical, thermal and geometric parameters.

In summary, for ensuring adequate operational flight safety, we have quantified the uncertainty involved in lightning strike damage probabilistically accounting for the effect of inevitable stochasticity in the material and geometric parameters. This will allow us to develop an improved optimum design paradigm through inclusive analysis and modeling of aircraft structures considering probabilistic information to avert structural failure and further assessment of residual structural performance incorporating the notion of reliability.

Declaration of competing interest

The authors declare that they have no known competing financial interests or personal relationships that could have appeared to influence the work reported in this paper.

Data availability

Data will be made available on request.

Acknowledgements

RSC acknowledges the financial support received through a doctoral scholarship from IIT Kanpur during the research work.

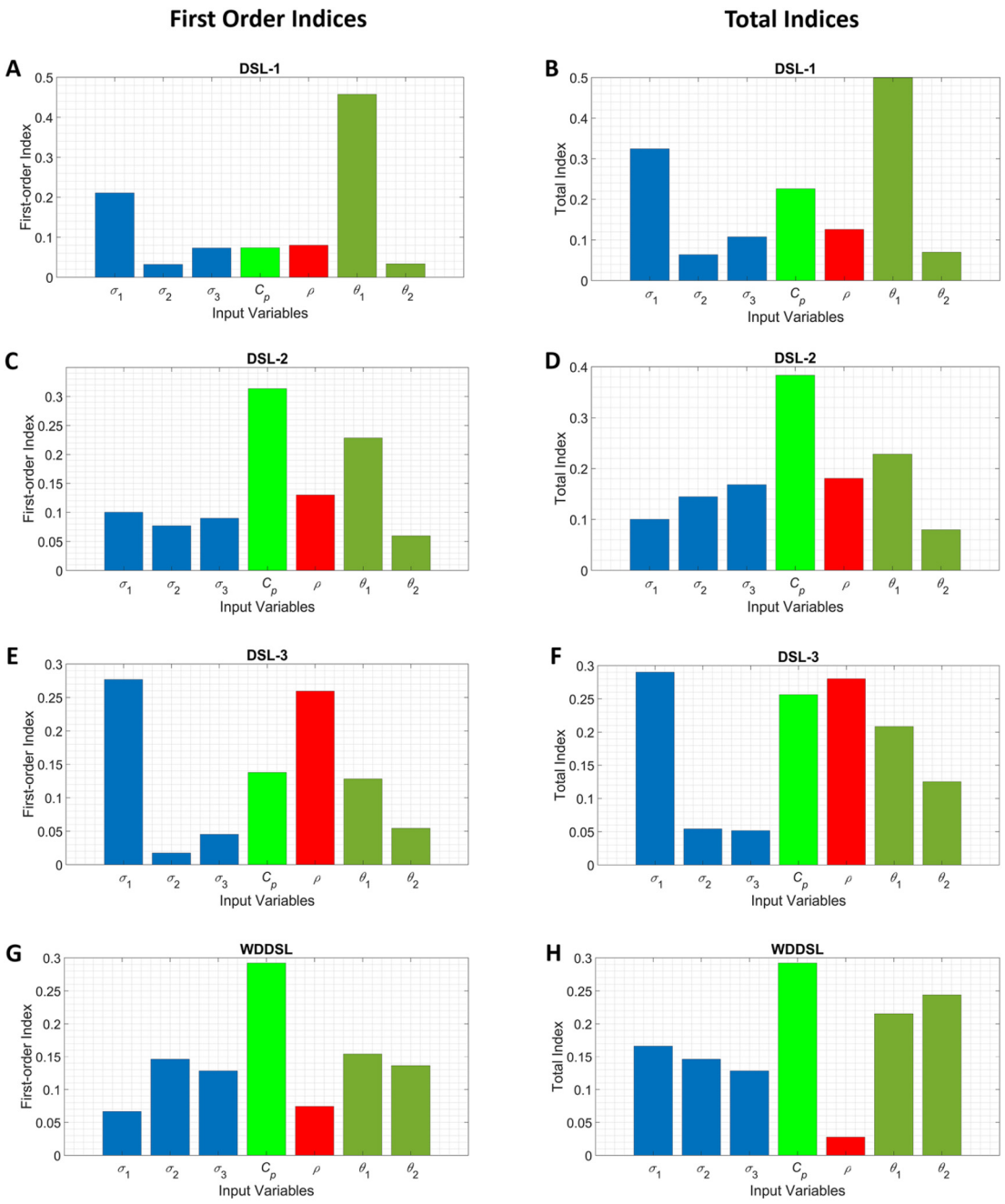

Fig. 16. Variance-based global sensitivity analysis for DSLs and WDDSL to understand the relative importance of the uncertain input parameters. (A, C, E) Ist order sensitivity indices for DSLs. **(B, D, F)** Total sensitivity indices DSLs. **(G)** Ist order sensitivity indices for WDDSL. **(H)** Total sensitivity indices for WDDSL.

References

[1] V. Kumar, T. Yokozeki, C. Karch, A.A. Hassen, C.J. Hershey, S. Kim, J.M. Lindahl, A. Barnes, Y.K. Bandari, V. Kunc, Factors affecting direct lightning strike damage to fiber reinforced composites: a review, Composites, Part B, Eng. 183 (2020) 107688.

[2] Y. Kim, J. Jo, D. Kim, H. Lee, R. Myong, Effects of lightning on UAM aircraft: complex zoning and direct effects on composite prop-rotor blade, Aerosp. Sci. Technol. 124 (2022) 107560.

[3] P. Feraboli, M. Miller, Damage resistance and tolerance of carbon/epoxy composite coupons subjected to simulated lightning strike, Composites, Part A, Appl. Sci. Manuf. 40 (6–7) (2009) 954–967.

[4] Y. Hirano, S. Katsumata, Y. Iwahori, A. Todoroki, Artificial lightning testing on graphite/epoxy composite laminate, Composites, Part A, Appl. Sci. Manuf. 41 (10) (2010) 1461–1470.

[5] Q. Dong, Y. Guo, X. Sun, Y. Jia, Coupled electrical-thermal-pyrolytic analysis of carbon fiber/epoxy composites subjected to lightning strike, Polymer 56 (2015) 385–394.

[6] T. Ogasawara, Y. Hirano, A. Yoshimura, Coupled thermal–electrical analysis for carbon fiber/epoxy composites exposed to simulated lightning current, Composites, Part A, Appl. Sci. Manuf. 41 (8) (2010) 973–981.

[7] S.L. Millen, J. Lee, Microscale modelling of lightning damage in fibre-reinforced composites, J. Compos. Mater. 57 (10) (2023) 1769–1789, https://doi.org/10.1177/00219983231163271.

[8] S. Millen, A. Murphy, Modelling and analysis of simulated lightning strike tests: a review, Compos. Struct. 274 (2021) 114347.

[9] J. Sun, X. Yao, W. Xu, J. Chen, Y. Wu, Evaluation method for lightning damage of carbon fiber reinforced polymers subjected to multiple lightning strikes with different combinations of current components, J. Compos. Mater. 54 (1) (2020) 111–125.

[10] B. Wang, Y. Zhu, Y. Ming, X. Yao, X. Tian, G. Ziegmann, Y. Duan, J. Sun, Understanding lightning strike induced damage mechanism of carbon fiber reinforced polymer composites: an experimental study, Mater. Des. 192 (2020) 108724.

[11] S. Arp, 5412: 2013, Aircraft Lightning Environment and Ralated Test Waveforms, SAE Aerospace, USA, 2013, pp. 1–56.

[12] S. Arp, 5416: 2013, Aircraft Lightning Test Methods, SAE Aerospace, USA, 2013, pp. 1–145.
[13] G. Abdelal, A. Murphy, Nonlinear numerical modelling of lightning strike effect on composite panels with temperature dependent material properties, Compos. Struct. 109 (2014) 268–278.
[14] Q. Dong, Y. Guo, J. Chen, X. Yao, X. Yi, L. Ping, Y. Jia, Influencing factor analysis based on electrical–thermal-pyrolytic simulation of carbon fiber composites lightning damage, Compos. Struct. 140 (2016) 1–10.
[15] F. Wang, Y. Ji, X. Yu, H. Chen, Z. Yue, Ablation damage assessment of aircraft carbon fiber/epoxy composite and its protection structures suffered from lightning strike, Compos. Struct. 145 (2016) 226–241.
[16] J. Lee, T.E. Lacy Jr., C.U. Pittman Jr., M.S. Mazzola, Thermal response of carbon fiber epoxy laminates with metallic and nonmetallic protection layers to simulated lightning currents, Polym. Compos. 39 (S4) (2018) E2149–E2166.
[17] J. Lee, T.E. Lacy Jr., C.U. Pittman Jr., M.S. Mazzola, Temperature-dependent thermal decomposition of carbon/epoxy laminates subjected to simulated lightning currents, Polym. Compos. 39 (S4) (2018) E2185–E2198.
[18] S. Shah, J. Lee, Stochastic lightning damage prediction of carbon/epoxy composites with material uncertainties, Compos. Struct. 282 (2022) 115014.
[19] A. Ameri, A. Fekrar, F. Bourada, M.M. Selim, K.H. Benrahou, A. Tounsi, M. Hussain, Hygro-thermo-mechanical bending of laminated composite plates using an innovative computational four variable refined quasi-3d hsdt model, Steel Compos. Struct. 41 (1) (2021) 31–44.
[20] H.D. Tahar, R. Abderezak, B. Rabia, A. Tounsi, Impact of thermal effects in frp-rc hybrid cantilever beams, Struct. Eng. Mech. 78 (5) (2021) 573–583.
[21] S. Dey, T. Mukhopadhyay, A. Spickenheuer, S. Adhikari, G. Heinrich, Bottom up surrogate based approach for stochastic frequency response analysis of laminated composite plates, Compos. Struct. 140 (2016) 712–727.
[22] S. Naskar, T. Mukhopadhyay, S. Sriramula, Probabilistic micromechanical spatial variability quantification in laminated composites, Composites, Part B, Eng. 151 (2018) 291–325.
[23] S. Dey, T. Mukhopadhyay, S. Adhikari, Uncertainty Quantification in Laminated Composites: a Meta-Model Based Approach, CRC Press, 2018.
[24] T. Mukhopadhyay, S. Naskar, P. Karsh, S. Dey, Z. You, Effect of delamination on the stochastic natural frequencies of composite laminates, Composites, Part B, Eng. 154 (2018) 242–256.
[25] G. Balokas, B. Kriegesmann, R. Rolfes, Data-driven inverse uncertainty quantification in the transverse tensile response of carbon fiber reinforced composites, Compos. Sci. Technol. 211 (2021) 108845.
[26] R.S. Chahar, T. Mukhopadhyay, Multi-fidelity machine learning based uncertainty quantification of progressive damage in composite laminates through optimal data fusion, Eng. Appl. Artif. Intell. 125 (2023) 106647, https://doi.org/10.1016/j.engappai.2023.106647.
[27] C.K. Williams, C.E. Rasmussen, Gaussian Processes for Machine Learning, vol. 2, MIT Press, Cambridge, MA, 2006.
[28] M. Raissi, G. Karniadakis, Deep multi-fidelity Gaussian processes, arXiv preprint, arXiv:1604.07484, 2016.
[29] I.M. Sobol, Uniformly distributed sequences with an additional uniform property, USSR Comput. Math. Math. Phys. 16 (5) (1976) 236–242.
[30] T. Mukhopadhyay, A multivariate adaptive regression splines based damage identification methodology for web core composite bridges including the effect of noise, J. Sandw. Struct. Mater. 20 (7) (2018) 885–903.
[31] J. Lee, T.E. Lacy Jr., C.U. Pittman Jr., Coupled thermal electrical and mechanical lightning damage predictions to carbon/epoxy composites during arc channel shape expansion, Compos. Struct. 255 (2021) 112912.
[32] J. Menousek, D. Monin, Laser Thermal Modeling of Graphite Epoxy, Naval Weapons Center Technical Memorandum, vol. 3834, 1979, p. 230.
[33] G.P. Mueller, The relative effects of cw and rp lasers on composites and metals, Tech. Rep., Naval Research Lab Washington DC, 1995.
[34] J.P. Fanucci, Thermal response of radiantly heated kevlar and graphite/epoxy composites, J. Compos. Mater. 21 (2) (1987) 129–139.
[35] C. Griffis, J. Nemes, F. Stonesifer, C. Chang, Degradation in strength of laminated composites subjected to intense heating and mechanical loading, J. Compos. Mater. 20 (3) (1986) 216–235.
[36] M.-C. Trinh, T. Mukhopadhyay, Semi-analytical atomic-level uncertainty quantification for the elastic properties of 2d materials, Mater. Today Nano 15 (2021) 100126.
[37] A. Mahata, T. Mukhopadhyay, M.A. Zaeem, Modified embedded-atom method interatomic potentials for al-cu, al-fe and al-ni binary alloys: from room temperature to melting point, Comput. Mater. Sci. 201 (2022) 110902.
[38] Y. Zhu, Y. Ming, B. Wang, Y. Duan, H. Xiao, C. Zhang, J. Sun, X. Tian, Finite element analysis of lightning damage factors based on carbon fiber reinforced polymer, Materials 14 (18) (2021) 5210.
[39] A. Sharma, T. Mukhopadhyay, S.M. Rangappa, S. Siengchin, V. Kushvaha, Advances in computational intelligence of polymer composite materials: machine learning assisted modeling, analysis and design, Arch. Comput. Methods Eng. 29 (5) (2022) 3341–3385.
[40] T. Mukhopadhyay, S. Naskar, S. Dey, et al., On machine learning assisted data-driven bridging of fsdt and hozt for high-fidelity uncertainty quantification of laminated composite and sandwich plates, Compos. Struct. 304 (2023) 116276.
[41] M. Awad, R. Khanna, Efficient Learning Machines: Theories, Concepts, and Applications for Engineers and System Designers, Springer Nature, 2015.
[42] S. Gupta, T. Mukhopadhyay, V. Kushvaha, Microstructural image based convolutional neural networks for efficient prediction of full-field stress maps in short fiber polymer composites, Def. Technol. 24 (2023) 58–82.
[43] A. Garg, T. Mukhopadhyay, M.O. Belarbi, L. Li, Random forest-based surrogates for transforming the behavioral predictions of laminated composite plates and shells from FSDT to Elasticity solutions, Compos. Struct. 309 (2023) 116756.
[44] A. Garg, T. Mukhopadhyay, M.O. Belarbi, H.D. Chalak, A. Singh, A.M. Zenkour, On accurately capturing the through-thickness variation of transverse shear and normal stresses for composite beams using FSDT coupled with GPR, Compos. Struct. 305 (2023) 116551.
[45] Vaishali, T. Mukhopadhyay, S. Naskar, S. Dey, On machine learning assisted data-driven bridging of FSDT and HOZT for high-fidelity uncertainty quantification of laminated composite and sandwich plates, Compos. Struct. 304 (2023) 116276.
[46] Vaishali, T. Mukhopadhyay, P.K. Karsh, B. Basu, S. Dey, Machine learning based stochastic dynamic analysis of functionally graded shells, Compos. Struct. 237 (2020) 111870.
[47] C.C. Onyekwena, Q. Xue, Q. Li, Y. Wan, S. Feng, H.I. Umeobi, H. Liu, B. Chen, Support vector machine regression to predict gas diffusion coefficient of biochar-amended soil, Appl. Soft Comput. 127 (2022) 109345.
[48] A.J. Smola, B. Schölkopf, A tutorial on support vector regression, Stat. Comput. 14 (3) (2004) 199–222.
[49] T. Mukhopadhyay, S. Naskar, S. Chakraborty, P. Karsh, R. Choudhury, S. Dey, Stochastic oblique impact on composite laminates: a concise review and characterization of the essence of hybrid machine learning algorithms, Arch. Comput. Methods Eng. 28 (2021) 1731–1760.
[50] A. Sharma, T. Mukhopadhyay, V. Kushvaha, Experimental data-driven uncertainty quantification for the dynamic fracture toughness of particulate polymer composites, Eng. Fract. Mech. 273 (2022) 108724.
[51] T. Mukhopadhyay, R. Kumar, S. Dey, et al., Probing the multi-physical probabilistic dynamics of a novel functional class of hybrid composite shells, Compos. Struct. 262 (2021) 113294.
[52] B. Isanaka, T. Mukhopadhyay, R. Varma, V. Kushvaha, On exploiting machine learning for failure pattern driven strength enhancement of honeycomb lattices, Acta Mater. 239 (2022) 118226.
[53] A. Saltelli, Making best use of model evaluations to compute sensitivity indices, Comput. Phys. Commun. 145 (2) (2002) 280–297.
[54] A. Saltelli, M. Ratto, T. Andres, F. Campolongo, J. Cariboni, D. Gatelli, M. Saisana, S. Tarantola, Global Sensitivity Analysis: the Primer, John Wiley & Sons, 2008.
[55] S. Chakraborty, S. Dey, S. Adhikari, A critical assessment of Kriging model variants for high-fidelity uncertainty quantification in dynamics of composite shells, Arch. Comput. Methods Eng. 24 (2017) 495–518.
[56] R.B. Tezel, Performance analysis of higher order statistical features in classification of some modulation types, Master's thesis, Fen Bilimleri Enstitüsü, 2020.
[57] M. Elangovan, V. Sugumaran, K. Ramachandran, S. Ravikumar, Effect of SVM kernel functions on classification of vibration signals of a single point cutting tool, Expert Syst. Appl. 38 (12) (2011) 15202–15207.
[58] C. Savas, F. Dovis, The impact of different kernel functions on the performance of scintillation detection based on support vector machines, Sensors 19 (23) (2019) 5219.
[59] D. Jahed Armaghani, Y.Y. Ming, A. Salih Mohammed, E. Momeni, H. Maizir, Effect of SVM kernel functions on bearing capacity assessment of deep foundations, J. Soft Comput. Civ. Eng. 7 (3) (2023) 111–128.
[60] J. Lee, T.E. Lacy Jr., C.U. Pittman Jr., M.S. Mazzola, Comparison of lightning protection performance of carbon/epoxy laminates with a non-metallic outer layer, J. Reinf. Plast. Compos. 38 (7) (2019) 301–313.